ULTRAMAFIC K-ALKALINE AND CARBONATITIC ROCKS FROM PLANALTO DA SERRA, MATO GROSSO, BRAZIL

A. De Min[1], P. Comin-Chiaramonti[1*], C.B. Gomes[2], .A.V. Girardi[2], F. Slejko[1], E. Ruberti[2]

[1]Mathematics and Geosciences Department, Trieste University: Via Weiss 8. I-34127 Trieste, Italy.
[2]Instituto de Geociências, University of Sao Paulo, Cidade Universitária, Rua do Lago, 562, 05508-900 São Paulo, Brazil.
[*]Corresponding author: e-mail: comin@unit.it

ABSTRACT

The Planalto da Serra lithotypes are represented by 600 Ma plugs and necks of glimmerites and carbonatites. Phlogopite and/ or tetraphlogopite are the most abundant minerals of the glimmerites. Carbonatites comprise granular hypidiomorphic alvikites and brecciod beforsites. Diopside and melanitic garnet are restricted to the glimmerites, whereas pyroclore occur only in carbonatites. Perovskite, tremolite, magnetite, pyrite, apatite, titanite, chlorite and serpentine are common accessories of both lithologies. Under high CO_2 and H_2O activity glimmerites and carbonatites gave rise to hydrotermalites, in which chlorite and serpentine are the predominant minerals (up to 70%).They derived from tremolite, diopside and sometimes from olivine. Pyrite is a common accessory. Glimmerites, alvikitic dykes and hydrotermalites have kamafugitic affinity. Sr-Nd isotopes and incompatible trace-element data, characterized high LREE/HREE fractionation suggest that the K-ultramafic alkaline and carbonatite rocks originated from a varied metasomatized source mantle, characterized by Sr radiogenic enrichment. Crustal contamination is negligible or absent. Geochronological data of the Planalto da Serra rocks and its relationship with the low-grade metamorphic rocks of the Cuiabá Group make improbable the presence of the Clymene Ocean in this area. The age determination also rules out the geochronological relationship between the Planalto da Serra intrusions and the Mesozoic alkaline bodies from the Azimuth 125° lineament, and makes possible to relate its emplacement with to one of the most important extensional periods of Neoproterozoic times, which is characterized by the separation of Laurentia and the Amazonian Craton. The TDM model ages suggest that the Planalto da Serra melts derived from the remobilization of subcontinental lithospheric mantle that had been enriched by small-volume K-rich melt fractions at the Early to Late Neoproterozoic, which makes highly improbable the hypothesis of mantle plume tail, given that a subcontinental mantle enrichment, controlled by an Early Neoproterozoic event, produced similar ultramafic alkaline products at 600 and 80-90 Ma.

INTRODUCTION

Neoproterozoic rocks are found at the southern margin of the Amazonian Craton. They belong to the Paraguay Belt (PB, Fig. 1A), a tectonic feature crossed by the Azimut 125° lineament after Bardet (1977) and along which some important Brazilian alkaline provinces of Mesozoic age also occur (Fig. 1B).

The Paraguay belt (Fig. 2) is geographically divided by Neogene sediments of the Pantanal Basin into two segments named northern and southern Paraguay Belt (Alvarenga et al., 2010). The first segment was developed during the Brasiliano Cycle (Boggiani and Alvarenga, 2004; Manzano et al., 2008) and your stratigraphy mainly consists of the following groups: 1) a lower unit, i.e. the Cuiabá Group (850-630 Ma), which comprises the Nova Xavantina metavolcanic-sedimentary Formation and eight low-grade metasedimentary units; 2) carbonatic rocks of the Araras Group (about 580 Ma); 3) four low-grade metasedimentary formations of the Alto Paraguay Group (590-545 Ma), i.e. the upper unit (Lacerda Filho et al., 2004; Riccomini et al., 2007; Alvarenga et al., 2010).

More recently, the Paraguayan Belt was interpreted as linked to the closing of the Goiás-Pharusian Ocean, due to successive continental collisions, dated roughly between 600 and 650 Ma, which sutured the West African Craton against the Saharan Metacraton in the north, and the Amazonian against the São Francisco Craton in the south (Cordani et al., 2012). Several Brasiliano-Pan African orogenic belts were created in this process and are aligned along a very long area of South America and Africa (more than 6000 Km long) dominated by one of the major tectonic elements of the world, the Transbrasiliano-Kandi lineament (cf. Fig. 1 and Fig. 3 of Cordani et al., 2012).

In particular, at the northeastern side of the northern Paraguay Belt, i.e. in the Planalto da Serra region, some ultramafic and carbonatitic rocks occur intruding low-grade metasedimentary rocks of the Cuiabá Group along the Rio dos Cavalos Rift (Figs. 3 and 4, and Alvarenga et al., 2010).

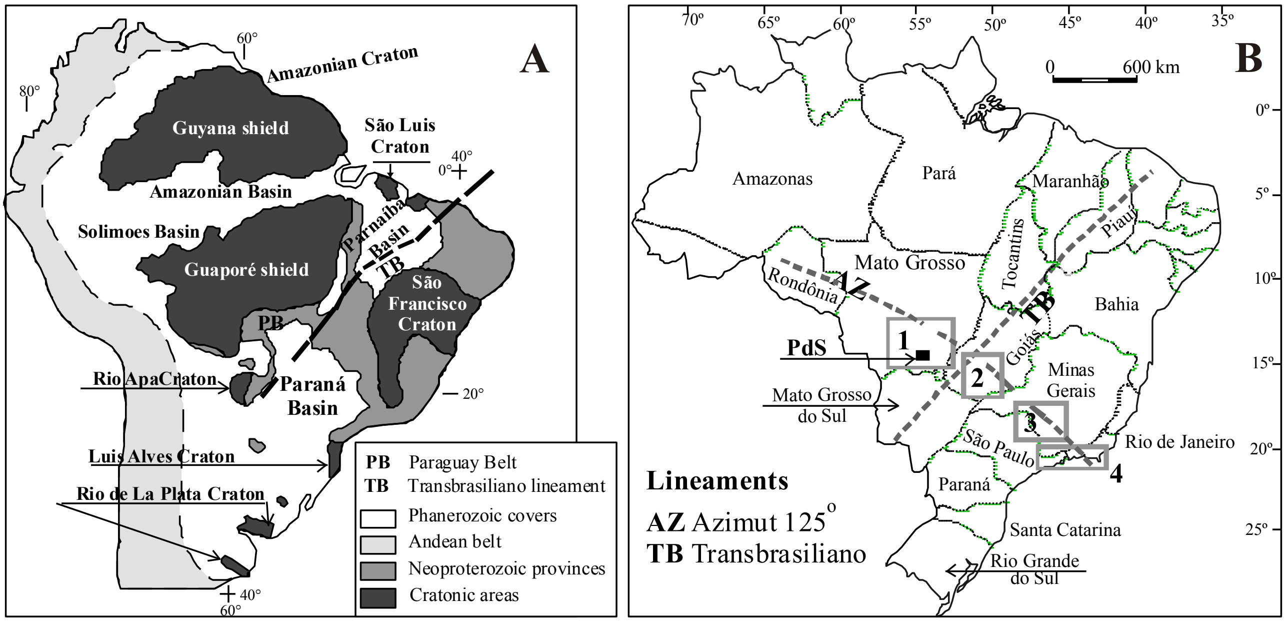

Fig. 1. A) Map of South America (modified after Almeida and Hasui, 1984, Heinz et al., 2005 and Cordani et al., 2009) showing cratonic areas, Neoproterozoic provinces and Phanerozoic covers. PB, Paraguay Belt; TB, Transbrasiliano huge continental shear zone (or a mega-suture). B) Two main Brazilian lineaments, Transbrasiliano and Azimut 125° (after Bardet, 1977, and Biondi, 2005), the latter including the alkaline provinces of 1, Poxoréu (age 84 Ma); 2, Rio Verde-Iporá and Goiás (age 80-90 Ma); 3, Alto Paranaíba (age 85 Ma); 4, Serra do Mar (age 85-55 Ma), according to Gibson et al. (1995, 1997).

THE PLANALTO DA SERRA INTRUSIVE SUITE: GEOLOGIC OUTLINES.

The Planalto da Serra K-alkaline ultramafic and carbonatitic rocks are located at the central part of the South American Plate, lying to Northeast of the city of Cuiabá in Mato Grosso state, western Brazil (Fig. 3). They represent some of the numerous bodies cropping out near the Azimut 125° lineament (cf. Biondi 2005), around the margins of the Paraná Basin (Comin-Chiaramonti and Gomes, 2005). These rocks were emplaced during Late Neoproterozoic, along a NE-SW trending extensional zone, the Rio dos Cavalos Rift (cf. Fig. 4, and De Min et al., 2012). This rift was developed between the northeastern part of the Paraná Basin and the southeastern margin of the Amazonian Craton, within the Late-Proterozoic Paraguay mobile belt (cf. Figs. 2 and 3).

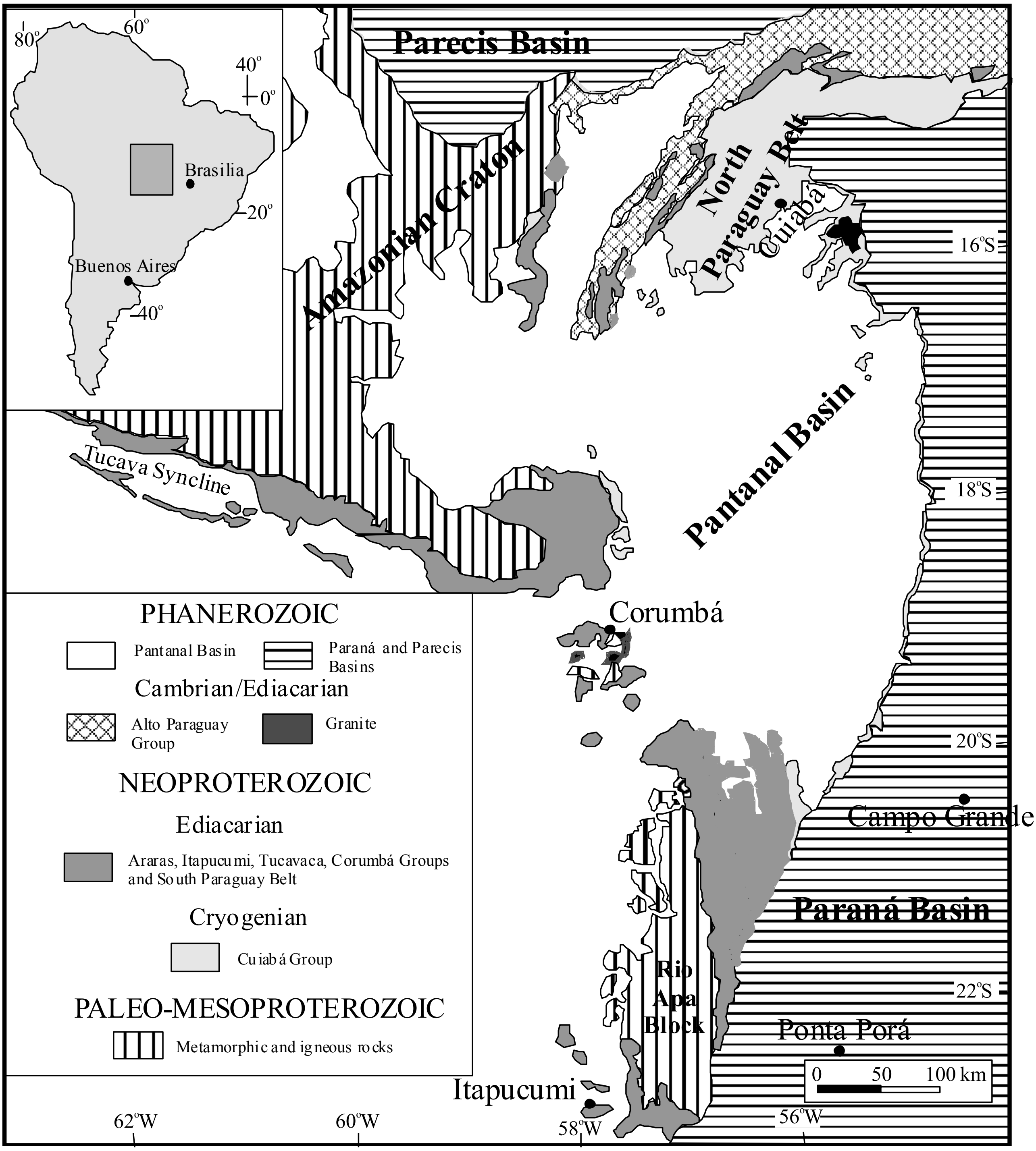

Fig. 2. Simplified geological map of the region including the Paraguay Belt (after Alvarenga et al., 2010, modified, cf. Dantas et al., 2007). To be noted that the São Vicente granite shows an age of 518±4 Ma (McGee et al., 2012).

The rock types from the Planalto da Serra are represented by dykes, plugs and breccioid necks (diatremes) of glimmeritic and carbonatitic affinity. Although the regional metamorphism of greenshist facies, which is associated with the end of the Brasiliano Orogeny (540-520 Ma, cf. Trindade et al., 2003) or being as late as 490 Ma (cf. Tohver et al., 2010), may have changed their original mineralogy, the age of the Planalto da Serra rocks is well constrained at about 600 Ma on the basis of Ar-Ar radiometric determinations carried out on phlogopite (De Min et al., 2012).

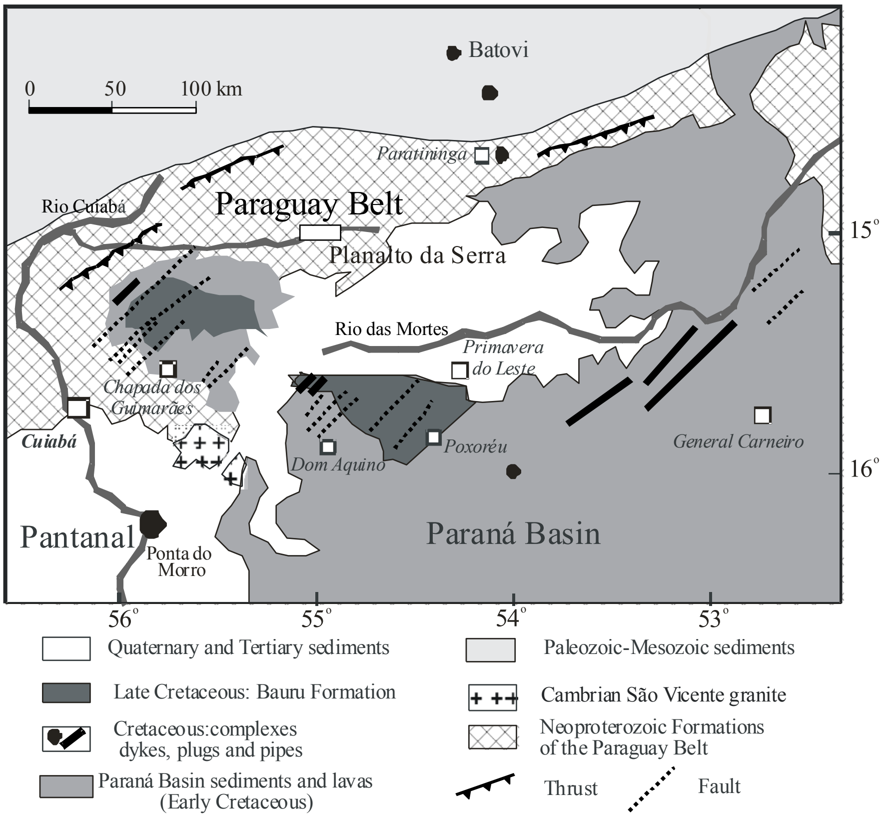

Fig. 3. Geological setting of the Mato Grosso State, after Sousa et al. (2005), showing part of the northern Paraguay belt and the the Planalto da Serra area.

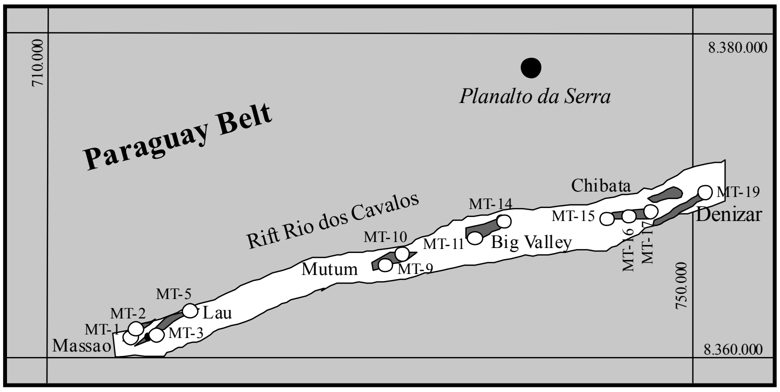

Fig. 4. Sketch map showing the Planalto da Serra area and the Rio dos Cavalos Rift in the Paraguay Belt (Mato Grosso State). Ultramafic and carbonatitic outcrops (after Ormond, 2006) and analyzed samples are indicated.

PETROGRAPHY

Glimmeritic rocks

The term glimmeritic rocks is applied to ultramafic alkaline dykes and plugs in which phlogopite and/or tetraferriphlogopite are the most abundant mineral (Fig. 5 I-II). They are inequigranular rocks, with coarse to fine texture, made of prevailing phlogopite-tetraferriphlogopite (up to 60 vol%) and subordinate amphibole and/or clinopyroxene, magnetite and primary carbonate (calcite). Clinopyroxene (and sometimes phlogopite) appears partially or completely replaced by amphibole (Fig. 5). Accessories are apatite, titanite, perovskite, garnet and pyrite. Garnet can be an important phase (up to 15 vol.%) in some plugs. Chlorite and serpentine (replacing original olivine) may be present in the plugs as secondary accessories. Representative modal analyses are in Table 1A.

Table 1. Estimated modal mineral abundances of the main rock-types (vol.% and calculated out of 1000 counted points; tr: trace) from Planalto da Serra (for the localities cf. Fig. 4). A: glimmeritic rocks; B: carbonatitic types; C, hydrothermalitized samples. Glass*: isotropic material with n < 1.5 (opal?).

A	MT-1	MT-2	MT-3	MT-15	MT-16	MT-17
Glimmeritic rocks	Dyke	Dyke	Dyke	Plug	Plug	Plug
Sample/Locality	Massao	Massao	Massao	Chibata	Chibata	Chibata
Phlogopite	50	44	58	51	60	49
Calcite	8	15	6	3	2	2
Dolomite	-		-	-	-	-
Amphibole	24	15	18	-	-	-
Clinopyroxene	4	12	2	22	22	19
Magnetite	8	9	9	15	3	9
Apatite	3	3	3	4	4	4
Garnet	tr	tr	tr	tr	6	15
Titanite	tr	tr	tr	tr	tr	1
Perovskite	tr	tr	tr	1	3	1
Pyrite	tr	tr	1	tr	tr	tr
Chlorite	1	1	2	4-	-	-
Serpentine	2	1	1	-	-	-

B	MT-5	MT-11	MT-13	MT-14	MT-19	**C**	MT-9	MT-10
Carbonatitic rocks	Alvikitic	Beforsitic	Beforsitic	Beforsitic	Beforsitic		Carbonatated	Hydrothermalite
Sample/Locality	Dyke	Neck	Neck	Neck	Neck		Dyke	Dyke margin
	Lau	Big Valley	Big Valley	Big Valley	Denizar		Mutum	Mutum
Phlogopite	15	5	-4	3	9		29	3
Amphibole	20				14		24	20
Calcite	51	3			3		26	3
Dolomite	-	59	59	65	51			
Magnetite	4	7	4	10	6		9	8
Pyrite	tr	tr	tr	tr	5		4	4
Apatite	3	1	2	2	2		1	3
Titanite	tr	tr	tr	tr	2		3	2
Perovskite	2	tr	tr	tr	2		tr	1
Chlorite	5	4	2	tr			1	29
Quartz and glass*		15	20	8	4			
Serpentine		6	9	12			3	27
Pyrochlore?	tr	tr	tr	tr	1			

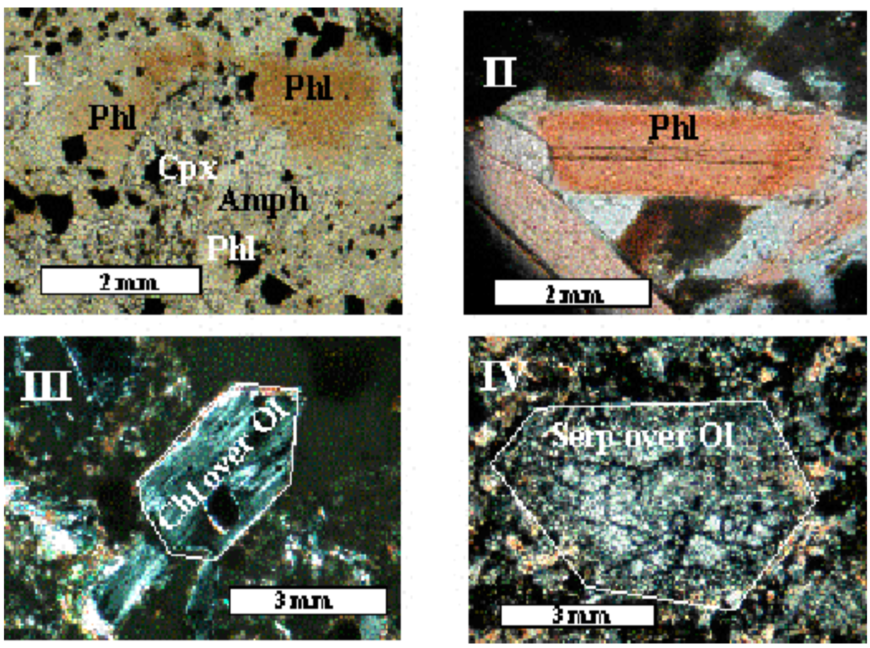

Fig. 5. I. MT-3 glimmeritic dyke (Phl, phlogopite ~ 50 vol%) showing clinopyroxene (Cpx) partially replaced by amphibole (Amph); N//. II. MT-16 glimmeritic plug characterized by tetraphlogopite (Phl, ~ 60 vol%); N//. III. MT-15 glimmeritic plug (Phl, ~ 51 vol%) with relicts of probable olivine (Ol) replaced by chlorite (Chl); N X**.** IV. MT-1 showing relicts of olivine (Ol) completely replaced by serpentine (Serp); N X.

Carbonatitic rocks

The characteristic feature of the alvikitic dykes (MT-5, Fig. 6.I) is its granular, hypidiomorphic, medium to fine-grained texture. The other carbonatites (cf. representative modal analyses of Table 1B) are beforsitic breccioid necks, coarse to medium-grained in texture. Euhedral to subhedral dolomite is predominant (Fig. 6.III), occurring associated with clasts of quartz and glass. Amphibole, phlogopite, apatite, opaque minerals (magnetite and pyrite), perovskite, pyrochlore and titanite constitute the complementary mineral assemblage. In few samples chlorite and serpentine pseudomorphs after mafic minerals are also observed (Figs. 6.II-IV). Phlogopite is normally euhedral, but can also form irregular and interstitial aggregates, sometimes in contact with opaque minerals and apatite. Perovskite is suhedral, in general disseminated in the rock, but in some samples is found as irregular aggregates in association with opaque minerals. Chlorite is present as interstitial fibrous aggregates, or as thin (millimetric) veins together with carbonates. Opaque minerals are represented by magnetite and pyrite. Pyrochlore is present in some samples, the grains being brownish, euhedral to subhedral and associated with apatite and opaque minerals. Some dykes are rich in primary carbonate (calcite up to 26 vol%) and have hydrothermalized chilled margins (cf. samples MT-9 and MT-10 of Table 1C) where clinopyroxene is completely uralitized.

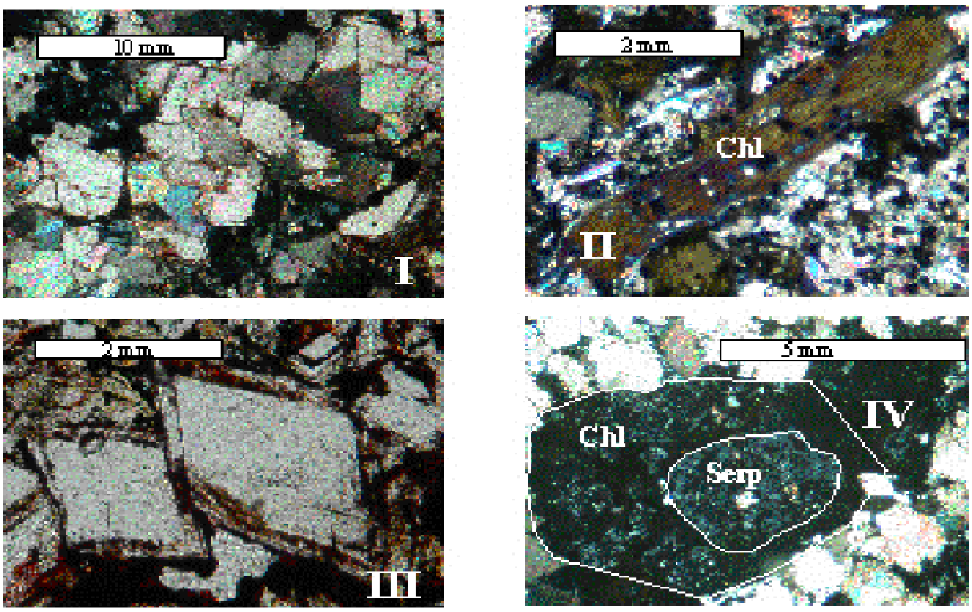

Fig. 6.I. MT-5 alvikite showing the calcite relationships; N X **II**. Chlorite (Chl) in MT-5 alvikite; N X. **III**. MT-11 beforsite showing euhedral dolomite crystals; N//. **IV**. Chlorite (Chl) and serpentine (Serp) pseudomorphs after mafic minerals in the MT-11 beforsite; N X.

Hydrothermalites

Some samples, i.e. MT-9 and MT-10 from Mutum dyke show a prevailing hydrothermal association of chlorite-serpentine-carbonate, and then may be defined as "hydrothermalites".

MINERAL CHEMISTRY

A systematic mineralogical investigation of the Planalto da Serra rocks was undertaken with the main aim of characterizing the typical minerals of the different assemblages. Microprobe analyses were carried out on polished sections at the São Paulo, Modena and Padova Universities, utilizing various equipments: at São Paulo, a JEOL model JXA-8600, having as analytical conditions 15 kV, 20 nÅ and beam diameter variable from 5 to 10 μm; at Modena, an ARL-SEMQ operating at 15 kV and 20 nÅ; at Padova, an energy dispersive spectrometer EDS EG 1G connected to a SEM AUTOSCAN microprobe operating at 15 kV. There a MAGIC program (ORTEC IV M version) was used to convert count rates into oxides wt%. On the whole oxides or simple silicate compounds were used as standards. The reported analyses are averaged by at least three point-analyses and the results are considered accurate within 2-3% for major elements and about 10% for the minor ones.

Phlogopite

Mica is a very important mineral of the Planalto da Serra rocks, being mainly represented by *phlogopite* and *tetraferriphlogopite.* The latter minerals occur as intercumulus primary phase, but can be also found as small aggregates of secondary origin, showing *chlorite* as the most common alteration product. Chemical analyses are reported in Table 2, with the structural formulae calculated assuming the positive charges balanced on 10 oxygen atoms and 2(OH+F+Cl) atoms; tetrahedral sites are believed to be completely filled by Si, Al and Ti to an occupancy of 4. Where the sum Si+Al+Ti is lower than 4.00 a.f.u., Fe^{3+} should be occupying the tetrahedral position. The octahedral sites are filled with Ti, Fe, Mg and Mn, whereas Na, K, Ca and Ba were assigned to the interlayered positions (cf. Brigatti et al., 2001).

Chemical analyses plotted on the conventional Al-Mg-Fe^{2+} diagram (Fig. 7A) show some overlapping for micas from the glimmeritic and carbonatitic rock types, with the phlogopite from carbonatites tending towards eastonite compositions. In general, early phlogopite can be found grading progressively into tetraferriphlogopite as a result of Al-deficiency during the magmatic crystallization. This particular feature has been also observed e.g. in other Brazilian alkaline-carbonatite occurrences (Araxá, cf. Traversa et al., 2001), kamafugitic and kimberlitic rocks from Alto Paranaíba, Brazil (Melluso et al., 2008) and in Uganda kamafugites (Scordari et al., 2012). Notably, the MT-9 and MT-10 dykes, display crystal rims strongly enriched in Ba, probably due to a highly localized influx of residual oxidized carbonatitic fluid (cf. Kopylova1et al., 2010).

Table 2. Representative chemical compositions of phlogopites from Planalto da Serra. Structural formulae calculated on the basis of 24(O,OH, F) and H_2O estimated assuming (OH, F)=4.000 a.f.u. Italics: analyses from Tab 5 of De Min et al. (2013).

SAMPLE	**MT-1**	***MT-3 Core***	***MT-3 Rim***	**MT-5**	**MT-9 Core**	**MT-9 Rim**	**MT-10 Core**	**MT-10 Rim**	***MT-16-Core***	***MT-16-Rim***	**MT-17**	**MT-19**
SiO_2	38.68	*38.97*	*37.59*	36.16	34.17	32.40	35.50	31.08	*38.89*	*37.99*	38.96	39.99
TiO_2	1.81	*2.82*	*3.90*	0.32	1.17	1.69	0.76	1.97	*2.10*	*2.13*	2.18	2.32
Al_2O_3	13.20	*12.81*	*14.09*	18.13	16.13	20.50	17.46	17.94	*11.55*	*11.67*	11.86	12.35
Fe_2O_3	1.41	*1.60*	*1.19*	4.92	0.00	0.00	3.01	0.00	*3.65*	*5.72*	4.74	4.86
FeO	9.70	*6.09*	*6.64*	1.22	4.03	1.83	3.22	4.62	*2.99*	*0.87*	2.17	2.66
MnO	0.21	*0.09*	*0.07*	0.10	0.05	0.05	0.16	0.04	*0.07*	*0.06*	0.05	0.02
MgO	20.37	*22.43*	*21.83*	25.07	24.86	23.82	23.35	23.49	*25.17*	*25.52*	24.80	23.70
CaO	0.03	*0.03*	*0.00*	0.07	0.05	0.05	0.18	0.02	*0.03*	*0.04*	0.06	0.10
BaO	0.00	*0.54*	*0.50*	0.16	6.66	9.32	1.08	11.18	*2.02*	*1.19*	1.33	0.79
Na_2O	0.13	*0.04*	*0.02*	0.04	0.06	0.47	0.07	0.15	*0.12*	*0.08*	0.13	0.18
K_2O	10.50	*10.47*	*10.10*	10.18	8.31	6.83	10.49	5.65	*9.77*	*10.26*	9.78	9.30
F	0.21	*0.19*	*0.06*	0.12	0.53	0.65	0.36	0.50	*1.09*	*1.51*	1.08	0.65
H_2O	3.75	*3.91*	*4.23*	3.51	2.98	2.39	4.05	4.36	*2.55*	*3.00*	2.88	3.08
Sum	100.00	*100.00*	*100.00*	100.00	100.00	100.00	100.00	100.00	*100.00*	*99.96*	100.02	100.00
afu												
Si	2.84	*2.82*	*2.72*	2.59	2.87	2.44	2.55	2.33	*2.72*	*2.71*	2.75	2.82
Al	1.14	*1.09*	*1.20*	1.41	1.13	1.56	1.45	1.59	*1.20*	*0.98*	1.08	1.05
Ti	0.02	*0.09*	*0.08*	0.00	0.00	0.00	0.00	0.08	*0.08*	*0.23*	0.10	0.00
Fe^{3+}	0.00	*0.00*	*0.00*	0.00	0.00	0.00	0.00	0.00	*0.00*	*0.08*	0.07	0.13
Sum	4.00	*4.00*	*4.00*	4.00	4.00	4.00	4.00	4.00	*4.00*	*4.00*	4.00	4.00
Al	-	-	-	0.02	0.18	0.16	0.03	0.00	-	-	-	-
Ti	0.08	*0.07*	*0.13*	0.02	0.06	0.09	0.04	0.03	*0.13*	*0.00*	0.08	0.13
Fe^{3+}	0.08	*0.10*	*0.09*	0.21	0.00	0.00	0.17	0.00	*0.09*	*0.23*	0.15	0.14
Fe^{2+}	0.60	*0.38*	*0.41*	0.07	0.23	0.11	0.20	0.31	*0.41*	*0.05*	0.21	0.16
Mg	2.23	*2.43*	*2.36*	2.67	2.55	2.65	0.01	2.64	*2.36*	*2.72*	2.55	2.57
Mn	0.01	*0.01*	*0.01*	0.01	0.00	0.00	2.55	0.00	*0.01*	*0.00*	0.01	0.00
Sum	3.00	*2.99*	*3.00*	3.00	3.02	3.01	3.00	2.99	*3.00*	*3.00*	3.00	3.00
Na	0.02	*0.01*	*0.00*	0.01	0.01	0.07	0.01	0.02	*0.00*	*0.01*	0.01	0.03
K	0.98	*0.97*	*0.93*	0.95	0.75	0.66	0.96	0.54	*0.93*	*0.94*	0.94	0.95
Ca	0.00	*0.00*	*0.00*	0.01	0.01	0.00	0.01	0.00	*0.00*	*0.01*	0.01	0.01
Ba	0.00	*0.02*	*0.02*	0.01	0.19	0.27	0.02	0.34	*0.02*	*0.04*	0.03	0.02
Sum	1.00	*1.00*	*0.95*	0.98	0.96	1.00	1.00	0.90	*0.95*	*1.00*	0.99	1.01
OH	1.84	*1.90*	*2.04*	1.68	1.40	1.20	1.90	2.18	*2.04*	*1.71*	1.80	1.64
F	0.05	*0.04*	*0.01*	0.04	0.12	0.16	0.25	0.12	*0.01*	*0.34*	0.16	0.15
O	10.11	*10.06*	*9.95*	10.28	10.48	10.61	9.85	9.70	*9.95*	*9.95*	10.04	10.21
Sum	12.00	*12.00*	*12.00*	12.00	12.00	12.00	12.00	12.00	*12.00*	*12.00*	12.00	12.00

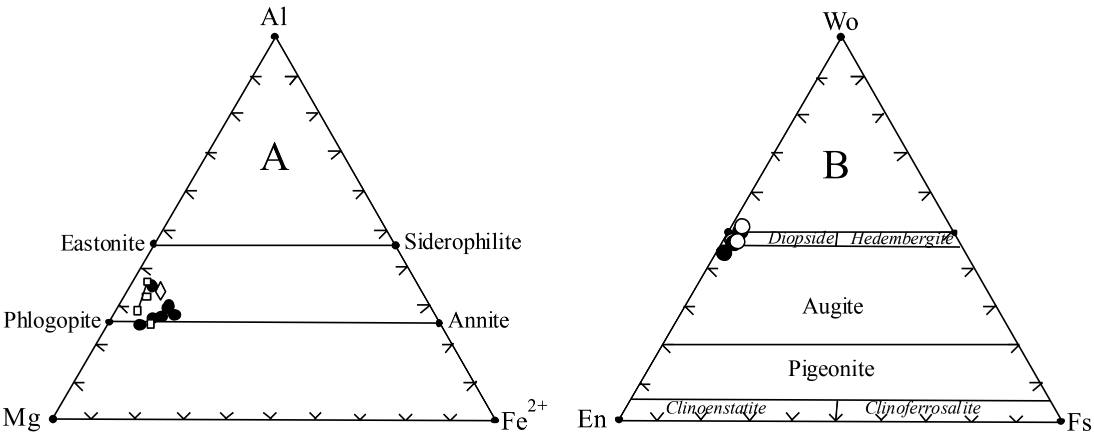

Fig. 7. A) Composition of micas plotted on the conventional Al-Mg-Fe diagram (Bailey, 1984). Full circles, glimmeritic rocks; open squares, carbonatitic rocks; open diamond, hydrothermalite. B) Clinopyroxene compositions (full circles, dykes; open circles, plugs) projected on the Wo-En-Fs ternary system. Nomenclature after Morimoto (1988).

Carbonates

Carbonate minerals correspond to 2-15 vol% of the whole composition of the glimmeritic rocks. Calcite shows low MgO and relatively high SrO (0.38-1.52 wt%), whereas dolomite is the main constituent of the beforsitic rocks (cf. Tables 1 and 3). In the MT-5 alvikitic sample the calcite content can reach up to 51% (Table 1). Other carbonate phases as ankerite, siderite, strontianite and magnesite were not observed. REE carbonates as primary or secondary phases may be also present (ΣREE up to 192 ppm in carbonatic phases). Notably in MT-19 sample, dolomite (51 vol%) coexists with exsolved calcite (3 vol%).

Table 3. Average microprobe analyses of carbonates. CO_2 calculated as from stoichiometry. The end members are also reported (wt%).

SAMPLE	MT-1	MT-2	MT-3	MT-5	MT-9	MT-10	MT-11	MT-13	MT-14	MT-15	MT-16	MT-17	MT-19	MT-19
FeO	0.37	0.21	0.19	0.06	0.05	0.37	0.27	0.27	0.28	0.07	0.22	0.29	0.07	0.29
MnO	0.17	0.25	0.43	0.16	0.01	0.23	-	0.01	-	0.02	0.13	0.21	0.02	-
MgO	1.22	0.59	0.34	0.22	0.01	0.45	18.84	20,35	21.10	0.10	0.28	0.47	0.12	21.85
CaO	52.87	54.19	54.56	55.13	55.69	54.73	33.68	31.91	31.02	55.11	55.03	54.53	55.50	30.13
SrO	1.52	1.10	1.23	0.54	0.84	0.38	0.03	0.04	0.05	1.34	0.86	0.93	1.34	0.06
BaO	0.05	0.03	0.03	0.02	0.04	0.05	-	-	-	0.17	0.11	0.04	0.17	-
CO_2	43.80	43.92	44.09	43.86	44.11	43.98	47.17	47.43	47.55	44.16	47.68	43.96	44.35	47.68
Sum	100.00	100.29	100.87	99.99	100.75	100.19	99.99	100.01	100.00	100.97	100.01	100.40	101.57	100.01
End members wt%														
Calcite	94.35	96,12	96.53	98.39	98.66	97.49	-	-	-	97.51	97.50	96.92	97.51	-
Siderite	0.87	0.74	0.99	0.35	0.08	0.97	-	-	-	0.14	0.56	0.67	0.14	-
Magnesite	2.55	1.24	0.70	0.46	0.02	0.94	-	-	-	0.25	0.58	0.98	0.25	-
Strontianite	2.17	1.56	1.74	0.77	1.19	0.54	-	-	-	1.88	1.21	1.33	1.88	-
Witherite	0.06	0.04	0.04	0.03	0.05	0.06	-	-	-	0.22	0.14	0.05	0.22	-
Dolomite	-	-	-	-	-	-	100.00	100.00	100.00	-	-			100.00

Clinopyroxenes

Clinopyroxenes, diopsidic in composition (Table 4 and Fig. 7B), occur only in the glimmeritic rocks. In the dykes (e.g. MT-3) the mineral is found as relict crystals in association with amphibole, phlogopite and carbonates (cf. Fig. 5.I); on the other hand, cumulus diopside is present in the plugs. Notably, in the carbonatitic rocks, ghosts of clinopyroxene appear to be completely replaced by amphibole and/or chlorite/serpentine.

Table 4. Representative microprobe analyses of clinopyroxenes in glimmeritic rocks. Total Fe was partitioned to Fe_2O_3 and FeO assuming charge balance and a theoretical formula containing 4 cations and 6 oxygens.

Sample	MT-1	MT-2	MT-3	MT-15	MT-16	MT-17
SiO_2	55.37	55.41	54.24	55.25	53.82	54.96
TiO_2	0.02	0.22	0.26	0.10	0.08	0.10
Al_2O_3	0.08	0.10	0.35	0.09	0.09	0.09
Cr_2O_3	0.06	0.10	0.06	0.09	0.11	0.09
Fe_2O_3	1.60	0.59	0.78	1.21	1.42	1.20
FeO	-	1.20	1.59	0.40	-	0.40
MnO	0.14	0.10	0.07	0.11	0.09	0.08
MgO	17.95	19.82	17.77	18.65	17.81	18.55
CaO	26.52	22.59	24.66	25.38	26.48	25.24
Na_2O	0.10	0.15	0.09	0.11	0.08	0.11
K_2O	-	0.06	0.00	0.03	0.02	0.03
Sum	101.83	100.28	99.97	101.41	100.00	100.05
a.f.u.						
Si	1.974	1.989	1.965	1.963	1.944	1.967
Al^{IV}	0.003	0.004	0.011	0.003	0.004	0.003
Ti	0.001	0.007	0.007	0.003	0.002	0.002
Fe^{3+}	0.043	0.000	0.017	0.031	0.050	0.028
Sum	2.000	2.000	2.000	2.000	2.000	2.000
Al^{VI}	0.000	0.000	0.004	0.000	0.000	0.000
Fe^{2+}	0.000	0.036	0.033	0.012	0.000	0.012
Mn	0.004	0.003	0.002	0.003	0.003	0.003
Mg	0.953	1.060	0.959	0.991	0.956	0.990
Fe^{3+}	0.021	0.016	0.029	0.012	0.000	0.012
Cr	0.002	0.003	0.002	0.002	0.003	0.002
Ca	1.013	0.869	0.965	0.971	1.031	0.971
Na	0.007	0.010	0.006	0.008	0.006	0.008
K	0.000	0.003	0.000	0.001	0.001	0.002
Sum	2.000	2.000	2.000	2.000	2.000	2.000
Atoms%						
Ca	50.3	44.2	48.9	48.4	50.5	48.5
Mg	47.3	53.8	48.5	49.4	46.9	49.5
ΣFe+Mn	2.4	2.0	2.6	2.2	2.6	2.0

Table 5. Representative microprobe analyses of amphiboles. Fe^{3+} and Fe^{2+} repartition according to Leake et al. (1997). Structural formulae calculated on the basis of 24(O,OH,F) and H_2O estimated assuming (OH,F)=2.000 a.f.u.

SAMPLE	MT-1	MT-2	MT-3	MT-5	MT-9	MT-10	MT-19
SiO_2	57.42	57.36	57.70	56.97	56.43	57.68	57.24
TiO_2	0.05	0.05	0.02	0.08	0.06	0.03	0.05
Al_2O_3	0.40	0.23	0.15	0.15	1.22	0.60	0.50
Fe_2O_3	1.24	0.91	1.48	0.00	1.16	0.43	0.86
FeO	1.78	2.44	2.51	3.03	4.03	1.53	2.58
MnO	0.13	0.16	0.18	0.16	0.25	0.20	0.18
MgO	23.04	23.08	22.98	23.22	21.41	23.31	22.79
CaO	13.63	13.38	13.64	12.87	12.79	12.67	13.12
Na_2O	0.20	0.20	0.19	0.21	0.27	0.28	0.23
K_2O	0.12	0.09	0.08	0.07	0.06	0.04	0.07
F	0.17	0.10	0.06	0.08	0.06	0.04	0.08
Cl	0.01	0.01	0.00	0.00	0.01	0.01	0.01
Sum	98.09	98.01	98.81	96.84	97.68	96.82	97.71
afu							
Si	7.869	7.903	7.865	7.975	7.885	7.947	7.908
Al	0.065	0.031	0.002	0.025	0.115	0.053	0.052
Ti	0.005	0.009	0.024	0.000	0.000	0.000	0.006
Fe^{3+}	0.061	0.057	0.109	0.000	0.000	0.000	0.034
Sum	8.000	8.000	8.000	8.000	8.000	8.000	8.000
Al	0.000	0.000	0.000	0.000	0.075	0.006	0.016
Ti	0.000	0.003	0.000	0.008	0.006	0.003	0.003
Fe^{3+}	0.067	0.037	0.044	0.000	0.061	0.045	0.042
Fe^{2+}	0.204	0.199	0.267	0.127	0.373	0.177	0.228
Mg	4.714	4.743	4.668	4.846	4.454	4.785	4.692
Mn	0.015	0.018	0.021	0.019	0.031	0.015	0.019
Sum	5.000	5.000	5.000	5.000	5.000	5.000	5.000
Fe^{2+}	0.000	0.019	0.019	0.039	0.036	0.000	0.019
Na	0.000	0.010	0.000	0.031	0.052	0.078	0.032
Ca	2.001	1.974	1.990	1.930	1.912	1.870	1.941
Sum	2.001	2.003	2.009	2.000	2.000	1.948	1.992
Na	0.053	0.043	0.050	0.026	0.021	0.000	0.030
K	0.023	0.017	0.014	0.013	0.011	0.008	0.013
Sum	0.084	0.60	0.064	0.039	0.033	0.008	0.043

Amphiboles

Amphiboles are mainly tremolitic in composition (Table 5) and usually replace the clinopyroxene. As matter of fact, in some glimmeritic samples diopside relicts can be found yet, but conversely in alvikitic dykes and in hydrothermalites the original clinopyroxene is completely substituted by tremolite.

Notably, the replacement of anhydrous by hydrous minerals is commonly used to infer infiltration of a rock by warm H_2O-rich fluids (cf. Welch and Pawley, 1991), as also suggested by the textural characteristics of the MT-10 hydrothermalite.

Table 6. Representative microprobe analyses of opaques. Fe_2O_3 and FeO (wt%), ulvöspinel (mol%) and end members calculated according to Carmichael (1967) and stoichiometry, respectively.

Sample	**MT-1**	**MT-2**	**MT-3**	**MT-5** Early	**MT-5** Late	**MT-9**	**MT-10**	**MT-11**	**MT-13**	**MT-14**	**MT-15**	**MT-16** Early	**MT-16** Late	**MT-17**	**MT-19**
SiO_2	0.18	0.23	0.28	0.17	0.17	0.13	0.23	0.33	0.29	0.30	0.30	0.06	0.51	0.31	0.32
TiO_2	11.80	10.90	10.00	1.03	4.02	0.98	4.52	8.07	6.36	7.21	6.48	11.03	0.34	8.45	7.85
Al_2O_3	2.52	1.30	0.07	31.37	0.08	0.03	1.38	2.73	1.95	2.34	1.74	2.47	0.02	2.12	2.15
Cr_2O_3	4.43	3.24	2.05	32.31	1.10	0.28	0.15	0.02	0.76	0.71	0.75	0.57	0.02	0.29	0.10
FeO_{tot}	73.70	77.36	81.02	17.25	83.76	89.70	85.98	82.26	84.02	83.54	83.82	74.76	91.47	80.71	83.97
MnO	2.51	2.03	1.55	0.25	0.53	0.19	0.16	0.13	0.73	0.30	0.13	5.27	0.32	2.49	0.45
MgO	0.25	0.22	0.19	16.82	0.22	0.40	0.82	1.23	0.97	1.10	0.87	0.96	0.42	0.98	1.25
ZnO	1.48	0.75	0.01	0.10	0.06	0.02	0.01	0.01	0.01	0.03	0.13	0.26	0.00	0.14	0.03
Sum	96.87	96.03	95.17	99.30	90.94	91.73	93.25	94.78	95.09	95.53	95.36	95.38	93.10	95.49	96.12
Fe_2O_3	36.39	41.69	46.99	0.56	56.69	65.50	57.56	49.90	53.79	51.78	53.13	44.51	67.19	35.69	37.17
FeO	40.95	39.84	38.72	16.74	32.74	30.75	34.18	37.35	35.60	36.95	36.06	34.70	31.01	50.03	51.86
Sum	100.51	100.20	99.86	99.35	96.61	98.28	99.01	99.77	100.66	100.72	100.73	99.83	99.83	100.50	101.18
afu															
Si	0.053	0.069	0.085	0.039	0.053	0.041	0.071	0.103	0.087	0.089	0.091	0.018	0.156	0.092	0.094
Ti	2.638	2.463	2.288	0.180	0.938	0.230	1.054	1.892	1.430	1.610	1.472	2.478	0.078	1.893	1.755
Al	0.883	0.454	0.025	8.606	0.029	0.011	0.504	1.002	0.686	0.819	0.619	0.870	0.007	0.744	0.726
Cr	1.041	0.773	0.505	5.947	0.270	0.069	0.037	0.004	0.181	0.167	0.180	0.135	0.005	0.068	0.023
Fe^{3+}	8.138	9.448	10.758	0.098	13.950	15.382	13.429	11.697	12.098	11.570	12.076	10.011	15.518	11.216	11.542
Fe	10.179	10.016	9.852	3.248	8.503	8.025	8.490	8.693	8.899	9.176	9.108	8.670	7.959	8.892	9.189
Mn	0.631	0.515	0.399	0.049	0.140	0.050	0.034	0.034	0.185	0.075	0.033	1.334	0.083	0.628	0.113
Mg	0.111	0.098	0.086	5.816	0.102	0.186	0.378	0.572	0.432	0.487	0.392	0.427	0.192	0.435	0.551
Zn	0.326	0.164	0.002	0.017	0.014	0.005	0.003	0.002	0.002	0.007	0.029	0.057	0.000	0.031	0.007
Sum	24.000	24.000	24.000	24.000	23.999	23.999	24.000	23.999	24.000	24.001	24.000	24.000	23.998	23.999	24.000
Mole%															
Ulvöspinel	43.03	40.95	38.87	3.65	20.69	4.97	19.41	32.00	25.96	28.65	26.69	40.40	4.35	33.12	30.98
Magnetite	39.98	46.96	53.94	-	74.74	91.76	75.83	61.47	66.97	64.95	68.15	39.90	92.27	54.71	61.60
Gahnite	3.46	1.74	0.02	0.19	0.17	0.07	0.03	0.02	0.02	0.07	0.33	0.63	-	0.34	0.07
Spinel	1.18	0.65	0.11	47.36	-	-	2.86	5.34	3.90	4.54	3.19	4.10	0.04	3.80	4.20
Hercynite	0.06	0.03	-	-	-	-	-	-	-	-	-	-	-	-	-
Chromite	5.55	3.71	1.87	31.14	1.58	-	-	-	-	-	-	0.48	-	-	-
Mg-chromite	-	0.41	0.83	17.12	-	0.42	0.63	0.03	1.04	0.94	1.03	-	0.03	0.38	0.13
Jacobsite	6.74	5.55	4.36	0.54	1.19	0.92	0.39	0.37	2.11	0.85	0.37	14.49	1.02	6.99	1.26
Mg-ferrite	-	-	-	-		1.86	0.85	0.77	-	-	0.24	-	2.29	0.66	1.76

Opaques

Pyrite is a common accessory phase in all the samples, being an important phase (content up to 4-5 vol%) only in hydrohermalitic samples (MT 9 and MT-10) and in the beforsitic neck MT-19 (cf. Table 1). Probably the mineral represents a later phase, as indicated in sample MT-10 where pyrite includes titanomagnetite having the same composition of the groundmass magnetite.

All the specimens contain titaniferous magnetite (ulvöspinel from 4 to 43 mol%; Table 6), the main differences being the Cr content (Fig. 8). In dykes and necks plus plugs, the Cr/(Cr+Al) ratios range from 0.5-0.9 to 0.0-0.4, respectively. Noteworthy, in the MT-5 alvikitic dyke, other than late Ti-magnetite, a subordinate xenocystals rich in spinel (47 mol%) and Mg-chromite (31 mol%, not shown in Fig. 8) is also present. Sometimes the magnetite is altered into hematite.

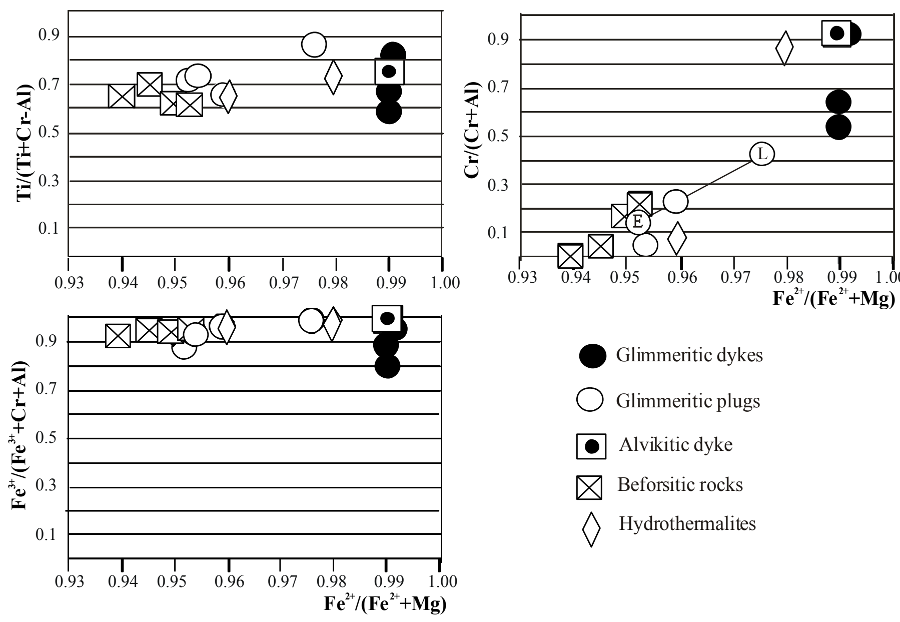

Fig. 8. $Fe^{2+}/(Fe^{2+}+Mg)$ vs.Ti/(Ti+Cr+Al), $Fe^{3+}/(Fe^{3+}+Cr+Al)$ and Cr/(Cr+Al) planes trough the spinel prism (Deer et al., 1992) illustrating magnetite variations in the Planalto da Serra specimens (cf. Table 6).

Garnet

Garnet is restricted to the glimmeritic rocks and constitutes an important phase only in the Chibata plug (MT16 and MT-17 samples: 6 and 15 vol%, respectively) and, subordinately, in the Massao dyke (MT-1: < 1vol%). It is brownish fine-grained and subidiomorphic to idiomorphic crystals. On the whole the mineral shows melanitic composition (Deer et al., 1992) and fits the equilibrium cooling trend of Kjarsgaard (1998) at temperature and pressure of 900°C and 0.2 GPa, respectively (Fig. 9).

Table 7. Representative microprobe analyses of garnets. Structural formulae on 24 oxygen basis and Fe_2O_3 as from charge balance.

	MT-1	**MT-15**	**MT-16**	**MT-17**
SiO_2	30.76	33.17	33.21	33.14
TiO_2	6.71	4.74	5.66	3.82
Al_2O_3	3.35	3.78	3.31	4.23
Cr_2O_3	0.25	0.07	0.05	0.06
Fe_2O_3	27,36	24.33	24.34	24.32
MnO	1.18	1.21	1.26	1.18
MgO	0.18	0.23	0.19	0.25
CaO	29.82	32.00	32.19	31.80
Na_2O	0.19	0.05	0.00	0.09
Sum	99.80	99.58	100.21	98.89
afu				
Si	5.195	5.554	5.529	5.579
Al	0.667	0.446	0.471	0.421
Ti	0.139	0.000	0.000	0.000
Sum	6.000	6.000	6.000	6.000
Al	0.000	0.299	0.179	0.418
Ti	0.713	0.597	0.709	0.484
Cr	0.033	0.009	0.007	0.008
Fe^{3+}	3.254	3.065	3.049	3.081
Sum	4.000	3.970	3.944	3.991
Fe^{2+}	0.223	0.000	0.000	0.000
Mn	0.169	0.174	0.178	0.169
Mg	0.045	0.060	0.047	0.063
Ca	5.496	5.740	5.742	5.738
Na	0.062	0.015	0.000	0.030
Sum	5.967	5.989	5.967	6.000
Al	16.9	16.9	14.7	19.0
Fe^{3+}	69.6	69.6	69.2	70.0
Ti	13.5	13.5	16.1	11.0

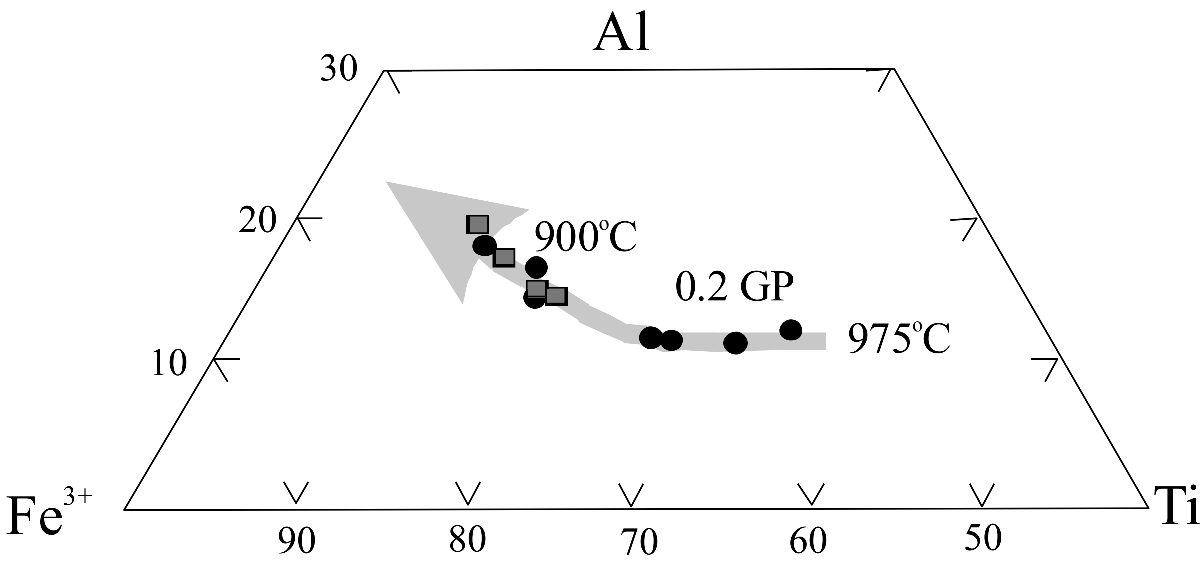

Fig. 9. Compositions of melanitic garnets (grey squares) from Planalto da Serra, as represented on the Al-Fe^{3+}-Ti triangular plot (atom%, cf. Table 7). Temperatures (°C) and equilibrium cooling trends at 0.2 GPa are also shown (cf. Kjarsgaard, 1998).

Perovskite and Nb-rich oxides.

Perovskite microphenocystals and microlites are ubiquitous and may be an important accessory phase (up to 2-3 vol%; cf. Table 1) in some glimmeritic and carbonatitic rocks (e.g. MT-5, MT-16 MT-19). Representative chemical analyses are reported in Table 8, from which appears possible to apply the oxygen barometer based on the Fe and Nb content of $CaTiO_3$ perovskite to estimate the oxygen fugacity (fO_2) during the crystallization and emplacement of the rock types (ΔNNO of Bellis and Canil, 2007, relative to the nickel-nickel oxide buffer). The ΔNNO values obtained for the Planalto da Serra rocks vary from 0.63 to 2.50. Notably, the Ca/Ti ratios are slighty over the unity (1.022±0.004 a.f.u.), and some quantity of REE (Σ=2.4-4.7 wt%), $(Nb,Ta)_2O_5$ (0.6-0.7 wt%), other than Th (up to 0.60 wt%) and Fe_2O_3 1.38-1.96 wt%) are present (cf. Boctor and Boyd, 1979). These results are very similar to those of fO_2 (ΔNNO) conditions for Lac de Gras pipes (Chakhmouradian and Mitchell, 2001; Canil and Bellis, 2007).

Table 8. Representative analyses of perovskites. Structural formulae on 3 oxygen basis. ΔNNO: oxygen barometer after Bellis and Canil (2007). The composition of Nb-rich oxides is also shown (pyrochlore?)

Sample	**MT-5**	**MT-15**	**MT-16**	**MT-19**		*a.f.u.*	**MT-5**	**MT-15**	**MT-16**	**MT-19**	**Nb-rich oxides**	**MT-5**	**MT-19**
SiO_2	0.12	0.06	0.00	0.26		Si	0.003	0.001	0.000	0.006	Nb_2O_5	65.53	63.27
TiO_2	52.19	53.63	55.07	54.29		Ti	0.926	0.938	0.950	0.942	Ta_2O_5	3.43	5.69
Th_2O	0.60	0.35	0.11	0.09		Th	0.007	0.004	0.001	0.001	TiO_2	1.56	2.15
Al_2O_3	0.31	0.30	0.30	0.29		Al	0.009	0.008	0.008	0.008	ThO_2	0.51	0.46
Fe_2O_3	1.96	1.67	1.38	1.51		Fe^{3+}	0.034	0.029	0.023	0.026	UO_2	0.02	2.16
Nb_2O_5	1.43	1.00	0.55	0.69		Nb	0.015	0.011	0.006	0.007	La_2O_3	0.17	0.11
Ta_2O_5	0.25	0.17	0.09	0.12		Ta	0.002	0.001	0.000	0.001	Ce_2O_3	0.26	0.26
MnO	<0.01	0.01	0.01	0.02		Mn	0.000	0.000	0.000	0.000	Y_2O_3	0.17	0.13
MgO	0.01	0.01	0.01	0.03		Mg	0.000	0.000	0.000	0.001	FeO	0.03	0.06
CaO	37.26	38.37	39.47	39.20		Ca	0.942	0.957	0.971	0.967	CaO	14.73	14.30
SrO	0.60	0.58	0.57	0.47		Sr	0.008	0.008	0.008	0.006	SrO	0.72	0.63
Na_2O	0.30	0.15	0.20	0.22		Na	0.014	0.011	0.009	0.010	PbO	0.00	0.03
La_2O_3	1.00	0.79	0.57	0.58		La	0.009	0.007	0.005	0.005	Na_2O	7.46	7.43
Ce_2O_3	2.42	1.90	1.37	1.39		Ce	0.021	0.016	0.012	0.012	F	5.50	4.66
Pr_2O_3	0.24	0.19	0.13	0.18		Pr	0.002	0.001	0.001	0.001	Sum	100.09	101.34
Nd_2O_3	0.82	0.65	0.48	0.65		Nd	0.007	0.005	0.004	0.005	O=F	2.32	1.96
Sm_2O_3	0.18	0.18	0.19	0.23		Sm	0.002	0.002	0.002	0.002	Sum	96.91	98.64
Sum	99.69	100.01	100.50	100.19		Sum	2.001	1.999	2.000	2.000			
						ΔNNO	0.63	1.57	2.50	1.88			

Nb-rich phases are present as accessory microlites (≤1 vol%) in the groundmass of the carbonatitic rocks. Representative chemical analyses relative to the MT-5 alvikitic and MT-19 beforsitic rocks are listed in Table 8 where the more abundant elements are Nb (Nb_2O_5 63-65 wt%), CaO (~14 wt%) and Na_2O (~7.4 wt%). On the basis of the Ti-Nb-Ta relationships these phases can be classified as pyrochlore (cf. Černy and Ercit, 1986). Similar compositions are reported by Simandl et al. (2001) for pyrochlore from Blue River carbonatites, British Columbia.

Titanite and apatite

Titanite and apatite are also ubiquitous accessory minerals and occur as microlites and more scarcely as microphenocrytals. Major element contents in titanite are relatively constant, i.e. SiO_2=29.8±0.3, TiO_2=36.2±0.5, CaO=26.1±0.3 wt% (cf. Table 9).

In apatite the following ranges in F and Sr contents were detected: F, 3-4.7 wt%; Sr, <0.1-0.3 wt%. Notably, these variations closely match those registered in Leucite Hills and in Paraguay apatites (Mitchell and Bergmann, 1991, and Comin-Chiaramonti and Gomes, 1995).

Secondary accessories

Secondary accessory minerals are mainly represented by chlorite and serpentine. They occur as alteration products of phlogopite and tremolite and are particularly abundant in the MT-10 hydrothermalite (chlorite 29 vol%, serpentine 27 vol%).

Sometimes chlorite and serpentine are found replacing original phases that have clearly the shape of olivine (cf. Figs. 5.III and 6.IV):

According to Tomkins et al. (1984), high calcium contents implies chloritization under high CO_2 activity. The chlorites are compositionally distinctive, high in SiO_2 and MgO and low in Al_2O_3, and plot inside the field of the chlorites of kimberlites from Sierra Leone (cf. Fig. 10). On the other hand, the diatreme facies, explosive and H_2O enriched (e.g. MT-10; cf. Table 1), resulted in the formation of serpentine+chlorite. Moreover, there are also textural evidences of transformation to serpentine of tremolite as a probable precursor.

Table 9. Representative microprobe analyses of titanites (a.f.u. on the basis of 4Si), and apatites: a.f.u. on the basis of 26(O,F).

Titanite	**MT-1**	**MT-9**	**MT-10**	**MT-17**	**Mt-19**		**Apatite**	**MT-1**	**MT-5**	**MT-15**	**MT-19**
SiO_2	29.66	30.23	29.53	29.77	30.00		SiO_2	0.37	0.53	0.12	0.42
TiO_2	35.80	36.96	35.74	36.08	36.54		TiO_2	0.01	0.02	0.00	0.01
ZrO_2	0.00	0.02	0.10	0.03	0.04		Al_2O_3	0.28	0.42	0.09	0.33
Nb_2O_5	0.39	0.57	0.72	0.52	0.59		MgO	0.01	0.00	0.01	0.00
Al_2O_3	2.15	2.14	2.37	2.20	2.20		CaO	54.55	53.89	55.44	54.33
Fe_2O_3	3.91	3.11	3.20	3.53	3.21		MnO	0.03	0.03	0-02	0.03
MnO	0.05	0.09	0.03	0.05	0.07		FeO	0.33	0.49	0.13	0.38
MgO	0.96	0.78	0.91	0.90	0.83		SrO	0.20	0.30	0.07	0.24
CaO	25.96	26.63	25.89	26.11	26.38		Na_2O	0.08	0.12	0.03	0.10
SrO	0.12	0.26	0.16	0.17	0.22		K_2O	0.01	0.01	0.00	0.01
Na_2O	0.10	0.06	0.08	0.08	0.07		P_2O_5	42.00	42.00	42.00	42.00
La_2O_3	0.18	0.37	0.11	0.21	0.29		F	4.36	4.67	3.03	4.28
Ce_2O_3	0.44	0.54	0.28	0.42	0.46		Sum	102.23	102.48	100.94	102.13
Sum	99.86	101.76	99.12	100.07	100.90		O=F	1.84	1.97	1.66	1.88
a.f.u.							Sum	99.71	99.78	99.57	99.73
Si	4.000	4.000	4.000	4.000	4.000						
Al	0.171	0.167	0.189	0.175	0.173		P	5.970	5.975	5.965	5.972
Fe^{3+}	0.198	0.155	0.163	0.178	0.161						
Ti	3.631	3.678	3.641	3.645	3.664		Ti	0.001	0.002	0.000	0.001
Zr	0.000	0.001	0.007	0.002	0.002		Al	0.056	0.084	0.019	0.202
Sum	4.000	4.001	4.000	4.000	4.000		Mg	0.001	0.000	0.001	0.000
							Ca	9.814	9.692	9.965	9.775
Mg	0.193	0.154	0.184	0.181	0.165		Mn	0.004	0.004	0.002	0.004
Nb	0.012	0.021	0.022	0.017	0.020		Fe	0.032	0.068	0.013	0.050
Mn	0.006	0.010	0.003	0.006	0-008		Sr	0.020	0.030	0.007	0.023
Na	0.013	0.008	0.010	0.011	0.009		Na	0.027	0.041	0.011	0.032
La	0.004	0.009	0.003	0.005	0.007		K	0.001	0.001	0.000	0.001
Ce	0.011	0.013	0.007	0.011	0.011		Sum	9.956	9.892	10.017	10.088
Sr	0.009	0.020	0.013	0.013	0.017						
Ca	3.751	3.772	3.758	3.758	3.766		F	2.316	2.484	2.091	2.371
Sum	3.999	4.007	4.000	4.002	4.003						

Table 10. Representative microprobe analyses of chlorites (a.f.u. on the basis of 28 O), and of serpentines (a.f.u. on the basis of 7 O).

Chlorite	**MT-3**	**MT-5**	**MT-10**	**MT-11**	**Serpentine**	**MT-10**	**MT-11**
SiO_2	32.65	31.91	33.30	32.23	SiO_2	41.30	41.69
TiO_2	0.21	0.15	0.20	0.31	TiO_2	0.06	0.07
Al_2O_3	9.13	8.74	9.32	8.99	Al_2O_3	0.55	0.57
FeO	18.98	22.69	16.26	17.87	Cr_2O_3	0.00	0.01
MnO	0.06	0.06	0.05	0.06	FeO	3.34	3.60
MgO	26.91	24.39	29.49	27.05	MnO	0.03	0.03
CaO	0.17	0.23	0.15	0.15	MgO	40.20	39.53
Na_2O	0.01	0.02	0.00	0.02	CaO	0.16	0.13
K_2O	0.12	0.04	0.15	0.12	Na_2O	0.00	0.01
Sum	88.24	88.23	89.10	86.80	K_2O	0.02	0.03
					NiO	0.01	0.01
					Sum	85.67	85.68
a.f.u.					***a.f.u.***		
Si	6.611	6.613	6.597	6.598	Si	1.971	1.989
Al	1.389	1.387	1.403	1.402	Al	0.029	0.011
Sum	8.000	8.000	8.000	8.000	Sum	2.000	2.000
Al	0.790	0.742	0.777	0.768	Al	0.002	0.021
Ti	0.032	0.024	0.030	0.048	Ti	0.002	0.003
Fe^{2+}	3.226	3.909	2.717	3.061	Cr	0.000	0.001
Mg	8.139	7.534	8.659	8.258	Fe^{2+}	0.133	0.144
Mn	0.007	0.007	0.006	0.011	Mg	2.862	2.813
Sum	12.194	12.215	12.189	12.146	Mn	0.001	0.001
					Na	0.000	0.001
Na	0.004	0.010	0.000	0.007	K	0.001	0.002
K	0.030	0.011	0.038	0.032	Ca	0.008	0.007
Ca	0.037	0.051	0.034	0.033	Ni	0.000	0.001
Sum	0.071	0.072	0.072	0.072	Sum	3.009	3.000

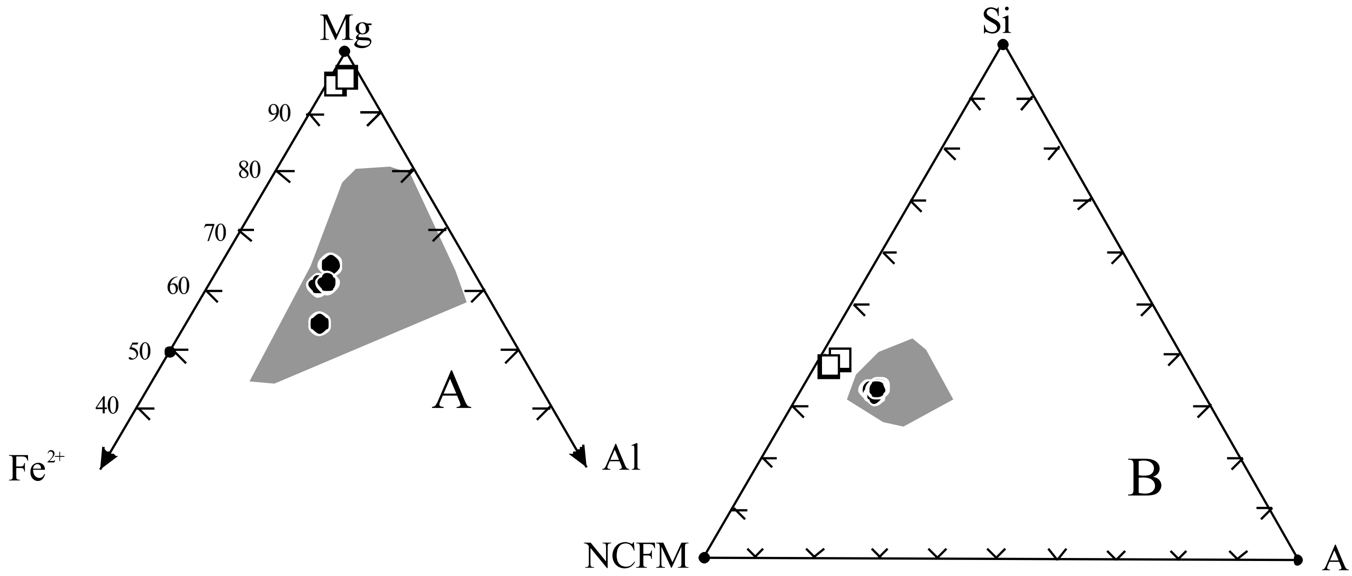

Fig. 10. **A:** Chlorite analyses plotted as a function of Mg-Fe^{2+}-Al. **B:** Si-NCFM(Fe^{2+}+Mg+Mn+Ca+2Na+2K-Ti)-A(Al+Fe^{3+}+Cr+2Ti), after Robinson et al. (1982). Variations of kimberlitic chlorites from Sierra Leone are also shown (grey fields; cf. Tomkins et al., 1984). Full circles, chlorites; squares, serpentines.

SIGNIFICANCE OF THE MINERALOGY

The mineralogy of the Planalto da Serra rocks when compared to other alkaline occurrences from the AZ 125° lineament (cf. Fig. 1) is, to some extent, similar to the Late Cretaceous glimmerites and carbonatites from APIP described by Gibson et al. (1995, 1997) and Thompson et al. (1998), for the following reasons: 1) the very abundant phlogopite, primary carbonates (cf. glimmerites, søvites and beforsites, after Gomes and Comin-Chiaramonti, 2005) and olivine; 2) the compositions of diopside, phogopite (tetraferriphlogopite), carbonates, opaques (titanomagnetite and chromium-spinel) and accessory apatite, titanite, perovskite and pyrochlore (cf. Bizzi and Araújo, 2005; Comin-Chiaramonti et al., 2005). The presence of primary melanitic garnet is indicative of equilibrium at 900°C and 2-5 Kb pressure (cf. Kjarsgaard, 1998). On the other hand, the presence of the tremolitic amphibole may be referred to hydratation, nucleation and growth of amphibole, accompanied by continuous dissolution of diopside at 800-850°C (about 5 Kb; cf. Welch and Pawley, 1991; Jenkins et al., 1991; Bozhilov et al., 2004). Finally, hydrothermal alteration affecting the pre-existing parageneses is responsible for the formation of chlorite, serpentine and pyrite.

PETROCHEMISRY

The glimmeritic rocks (Table 11, with major oxides wt% recalculated on a water-free basis) fit the kamafugitic field and/or the TAT (Toro-Ankole type) and II fields of Barton (1979) and Foley et al. (1987), respectively (Fig. 11). Even the glass in the beforsitic neck (MT-13) shows a kamafugitic affinity.

It is interesting to note that, on the basis of the classification shown by Fig. 11, the Planalto da Serra samples specifically refers to rock types considered ultrapotassic (i.e., $K_2O/Na_2O>2$, $K_2O>3$ wt% and MgO>3 wt%), plotting in the Toro Ankole Group (Group II of Foley et al., 1987) and that even the carbonatitic rocks can be considered to some extent as strongly potassic, having K_2O/Na_2O ratio 14.4±12.3 and K_2O 1.38±0.15.

On the whole the variation diagrams MgO vs. major oxides (Fig. 12) confirm the kamafugitic affinity of the non-carbonatitic samples.

Table 11. Chemical analyses of Planalto da Serra rocks. Major elements were analyzed by XRF fluorescence techniques using a PW1400 automatic spectrometer and pressed-powder pellets. FeO was determined by volumetric titration, using the ammonium metavanadate. Glass as taken from microprobe analyses. Glimm.: glimmeritic rocks. CO_2 and H_2O^+ were determined by wet chemical analyses (cf. also Galle and Runnel method, 1960). Italics: data from Table 1 of De Min et al. (2013).

Sample (locality)	**MT-1 (Massao)**	**MT-2 (Massao)**	***MT-3 (Massao)***	**MT-15 (Chibata)**	***MT-16 (Chibata)***	**MT-17 (Chibata)**	**MT-13 GLASS**
Rock type	Glimm. Dyke	Glimm. dyke	*Glimm. dyke*	Glimm. plug	*Glimm. Plug*	Glimmeritic Plug	In beforsitic neck
SiO_2	37.58	32.44	*37.36*	33.72	*32.65*	32.13	42.21
TiO_2	1.72	2.49	*3.06*	3.09	*2.99*	3.20	1.46
Al_2O_3	6.09	5.96	*6.84*	5.95	*6.62*	6.23	7.05
Fe_2O_3	2.15	1.86	*2.04*	1.93	*2.00*	2.09	3.33
FeO	9.83	9.28	*10.20*	9.63	*10.00*	10.45	6.84
MnO	0.20	0.20	*0.18*	0.21	*0.18*	0.23	0.15
MgO	17.26	18.46	*19.13*	15.88	*15.45*	16.05	18.55
CaO	12.42	13.57	*8.52*	17.58	*17.61*	17.72	10.39
Na_2O	0.13	0.05	*0.05*	0.23	*0.04*	0.04	1.00
K_2O	4.31	2.50	*3.41*	3.07	*3.27*	2.57	3.59
P_2O_5	1.20	1.33	*1.45*	1.75	*1.45*	1.53	0.76
S	0.09	0.03	*0.54*	0.04	*0.04*	0.06	-
CO_2	4.00	5.04	*2.18*	2.28	*1.07*	1.99	-
H_2O^+	2.41	4.86	*3.12*	4.40	*5.04*	5.49	-
Sum	99,28	98.07	*98.08*	99.76	*98.41*	99.78	95.33
CIPW Norm							
or	3.63-	-	*20.15*	-	-	-	0.01
ab	-	-	*0.42*	-	-	-	-
an	3.31	8.65	*8.37*	6.20	*8.23*	9.23	4.15
ne	0.60	0.23	-	1.95	*0.18*	0.18	4.58
lc	17.12	11.59	-	14.23	-	-	16.63
kp	-	-	-	-	*10.98*	8.79	-
di	20.16	12.15	*8.47*	5.47	*14.08*	14.21	33.58
ol	33.71	37.05	*38.72*	34.88	*31.42*	32.77	27.02
cs	-	2.53	-	14.73	*14.02*	12.13	-
mt	3.12	2.70	*2.96*	2.80	*2.90*	3.03	4.83
il	3.27	4.73	*5.81*	5.87	*5.68*	6.08	2.77
pr	0.19	0.06	*1.15*	0.08	*0.09*	0.13	-
ap	2.78	3.08	*3.36*	4.05	*3.36*	3.54	1.76
cc	9.10	11.46	*4.96*	5.19	*2.43*	4.23	-

Sample (locality)	**MT-5 (Lau)**	**MT-11 (Big Valley)**	**MT-13 (Big Valley)**	**MT-14 (Big Valley)**	**MT-19 (Denizar)**		**MT-9 (Mutum)**	**MT-10 (Mutum)**
Rock type	Alvikitic Dyke	Beforsitic neck	Beforsitic neck	Beforsitic neck	Beforsitic neck		Carbonataded dyke	Hydrotherm. dyke
SiO_2	22.05	25.30	27.08	11.87	31.18		27.08	36.16
TiO_2	2.23	1.79	1.19	1.51	2.10		2.61	2.83
Al_2O_3	5.15	1.82	1.63	3.94	3.46		5.79	4.07
Fe_2O_3	1.42	0.97	0.77	1.21	1.34		1.76	6.01
FeO	7.08	4.85	3.83	5.56	6.67		9.79	10.41
MnO	0.15	0.24	0.15	0.19	0.13		0.19	0.09
MgO	11.02	12.59	13.82	17.00	11.74		15.75	26.71
CaO	25.22	21.03	19.52	22.48	17.89		18.47	8.11
Na_2O	0.15	0.05	0.10	0.31	0.70		0.02	0.07
K_2O	1.92	1.61	1.35	1.31	1.45		2.41	0.28
P_2O_5	0.74	0.23	0.64	0.55	0.62		1.31	1.77
S	0.02	-	0.03	0.02	2.55		0.97	0.09
CO_2	17.34	28.90	27.85	32.30	18.00		8.21	1.39
H_2O^+	5.29	0.55	1.15	1.56	1.93		5.42	2.21
Sum	99.78	99.93	99.11	99.81	99.76		99.78	100.17
CIPW Norm								
Q	-	16.30	16.65	-	9.92		-	-
C		-	-	-	0.01		-	-
or	11.34	9.51	7.98	4.08	8.57		-	1.65
ab	0.02	0.43	0.18	-	5.92		-	0.59
an	7.71	-	0.01	5.82	1.98		8.59	9.97
ne	0.68	-	-	1.42	-		0.09	-
lc	-	-	-	2.56	-		11.17	-
di	2.35	-	3.88	3.00	18.76		2.21	7.83
hy	-	4,32	5.24	-	-		-	17.44
ol	24.90	-	-	8.16	-		34.89	39.05
cs	-	-	-	-	-		6.13	-
mt	2.68	1.41	1.12	1.75	1.94		2.55	8.71
il	5.53	3.40	2.26	2.87	3.99		4.96	5.37
pr	0.06	-	0.06	0.04	5.41		2.06	0.19
ap	2.25	0.53	1.48	1.27	1.44		3.03	4.10
cc	17.86	3.23	-	-	-		18.67	3.16
dolomite	-	57.60	58.36	67.68	37.72		-	-

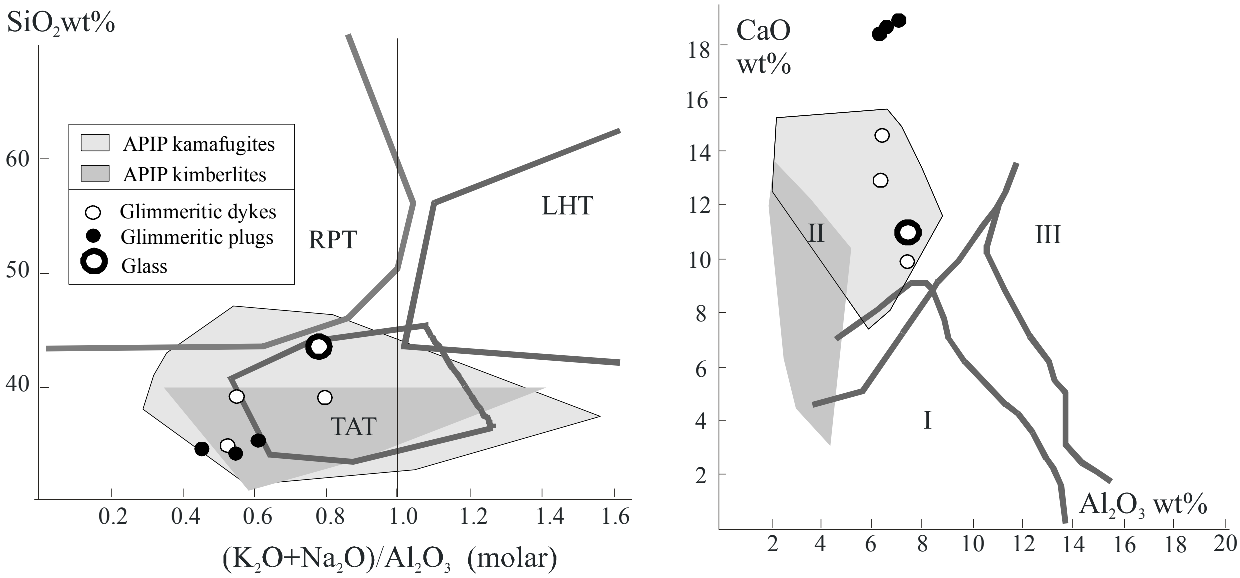

Fig. 11. Planalto da Serra rocks: molar $(K_2O+Na_2O)/Al_2O_3$ vs. SiO_2 (wt% on a water-free basis: LHT, Leucite Hills; TAT, Toro-Ankole; RPT, Roman Province lavas type after Barton, 1979) and CaO vs. Al_2O_3 (Group I, LHT; Group II, TAT; Group III, RPT; after Foley *et al.*, 1987) diagrams. APIP kamafugite and kimberlite fields are after Fig. 2 of Gomes and Comin-Chiaramonti (2005).

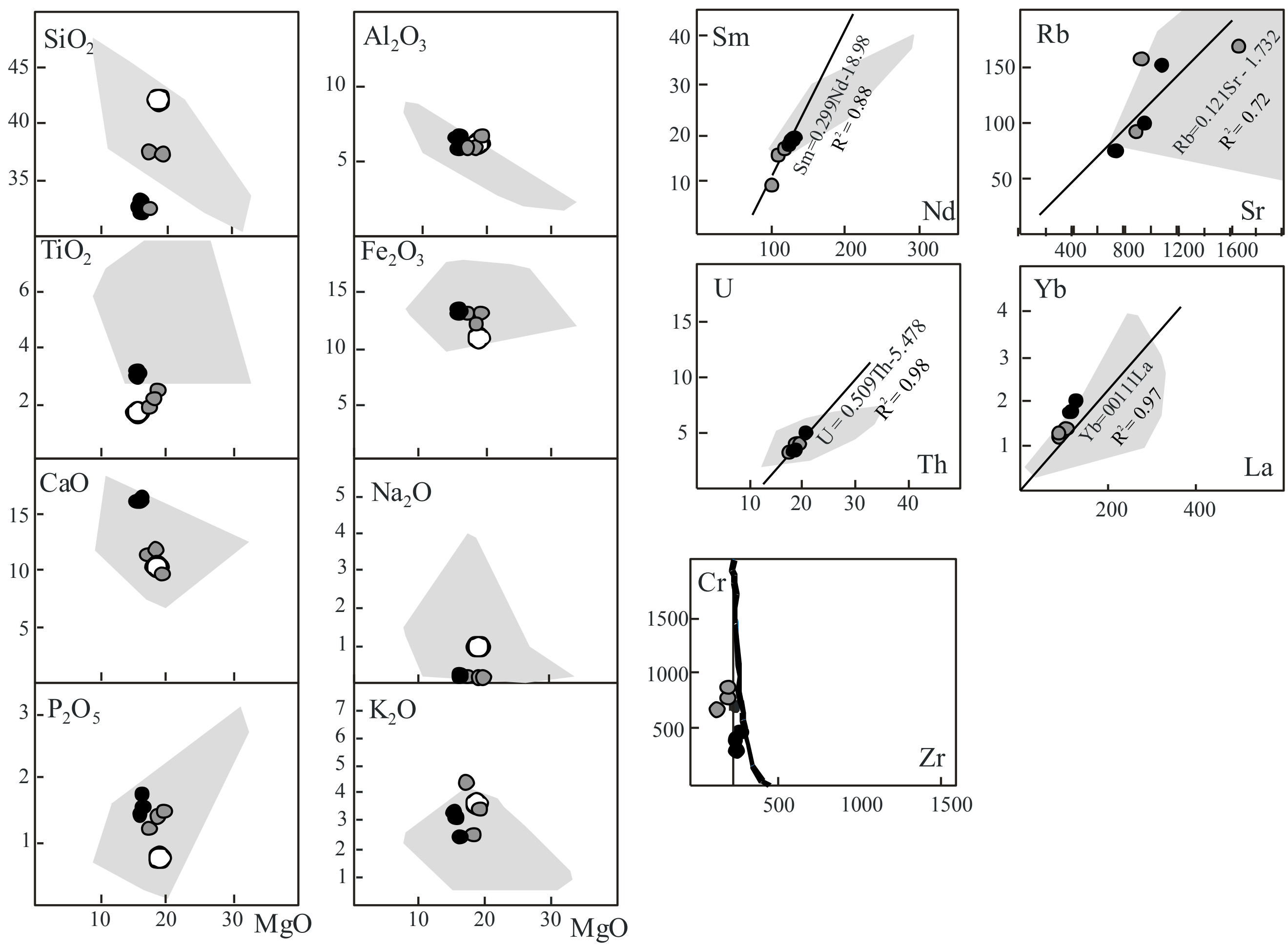

Fig. 12. MgO vs. major oxides and trace elements relationships, where the grey fields represent yhe APIP kamafugites. In the Zr vs. Cr diagram the heavy line represents the liquid descent of the APIP rock types (Zr_0=240; cf. Gomes and Comin-Chiaramonti, 2005). Symbols as in Fig. 11.

Table 12. Concentrations of trace elements of Planalto da Serra rocks (and carbonate fractions) determined by ICP-mass spectrometer at Actlabs (1336 Sandhill Drive, Ancaster, Ontario L9G 4V5; cf. Table 1). Italics: data from Table 1 of De Min et al:, 2013.

Sample ppm	**MT-1 (Massao)**	**MT-2 (Massao)**	***MT-3 (Massao)***	***MT-3 CF***	**MT-5 (Lau)**	**MT-5 CF**	**MT-9 (Mutum)**	**MT-10 (Mutum)**
Cr	753	664	*816*	-	876	-	342	274
Ni	628	575	*689*	-	601	-	359	328
Co	86.3	76	*94*	-	76.4	-	72.4	71.5
V	269	147	*236*	-	161	-	166	125
Ba	723	970	*1348*	*809.5*	541	503	1488	1220
Cs	19.2	24.0	*63.9*	*16.8*	2.6	0.61	1.2	2.0
Rb	58.5	187.6	*169.7*	*1.675*	71.9	1.60	21.8	18.0
Sr	909	1652	*940*	*6310*	1069	2732	1665	1219
Zr	215.0	169.9	*210*	*<0.03*	159.4	<0.03	220.4	314.3
Hf	4.8	4.2	*6.0*	-	3.9	-	5.8	7.1
Nb	140.3	130.9	*124.1*	*<0.01*	137.9	<0.01	182.1	252.1
Ta	8.2	6.9	*6.7*	-	6.2	-	7.7	8.5
Y	19.0	21.7	*21.1*	*3.74*	24.2	2.08	36.7	36.6
U	4.2	4.3	*3.4*	*0.68*	3.6	0.02	4.7	9.1
Th	19.1	19.4	*17.7*	*<0.01*	23.4	<0.01	38.2	40.9
Pb	12.7	7.0	*8.2*	*2.96*	1.6	<0.02	6.1	8.9
Cu	72.6	68.7	*89.2*	-	72.7	-	93.9	113.9
As	2.9	1.0	*7.5*	-	<0.5	-	15.0	1.8
Zn	49	62	*86*	-	27	-	138	99
Ga	14.7	12.0	*13.5*	-	11.7	-	12.5	13.9
La	118.1	136.9	*117.4*	*8.86*	149.5	10.57	248.1	316.2
Ce	252.8	286.0	*243.5*	*11.45*	307.9	13.05	448.9	546.5
Pr	27.53	31.82	*26.75*	*1.09*	33.87	1.44	46.69	54.55
Nd	105.7	118.9	*101.1*	*3.82*	126.5	5.36	165.4	194.7
Sm	15.42	16.23	*8.70*	*0.58*	15.09	0.62	23.29	20.27
Eu	4.15	4.31	*3.91*	*0.06*	4.9	0.09	6.3	6.62
Gd	10.66	10.24	*8.96*	*0.68*	12.19	0.51	15.34	16.64
Tb	1.23	1.21	*1.06*	*0.08*	1.36	0.04	1.77	2.00
Dy	5.31	5.18	*5.14*	*0.44*	6.18	0.24	8.3	9.29
Ho	0.73	0.77	*0.73*	*0.085*	0.81	0.04	1.21	1.26
Er	1.69	1.68	*1.63*	*0.22*	2.01	0.10	2.71	2.96
Tm	0.22	0.24	*0.21*	*0.02*	0.23	0.01	0.34	0.38
Yb	1.23	1.39	*1.24*	*0.15*	1.32	0.065	1.99	2.21
Lu	0.14	0.19	*0.17*	*0.02*	0.17	0.01	0.24	0.27

Sample ppm	**MT-11 (Big Valley 2)**	**Mt-11 CF**	**MT-13 (Big Valley 1)**	**MT-14 (Big Valley 2)**	**MT-15 (Chibata)**	***MT-16 (Chibata)***	***Mt-16 CF***	**MT-17 (Chibata)**	**MT-19 (Denizar)**	**MT-19 CF**
Cr	144	-	164	205	390	*383*	-	417	301	
Ni	153	-	140	232	368	*343*	-	364	270	
Co	26	-	40.2	30.3	66.7	*62.9*	-	73.8	45.8	
V	33	-	43	43	97	*113*	-	276	167	
Ba	51	27.4	123	49	1893	*1941*	*28.5*	1859	629	140
Cs	<0.1	0.055	0.2	0.1	3.0	*1.9*	-	4.7	1.0	0.06
Rb	18.3	0.45	0.4	18.2	75.5	*153.0*	*0.15*	99.3	18.5	0.46
Sr	200	194	242	195	739	*1067*	*195*	933	628	618
Zr	95.4	<0.03	115.4	148.4	232.6	*236.5*	-	267.3	203.5	<0.03
Hf	2.5	-	3.0	3.9	5.9	*6.5*	-	6.9	5.1	-
Nb	56.2	<0.01	67.4	80.0	143.7	*136.0*	-	153.5	77.7	0.01
Ta	2.2	-	2.6	3.1	7.6	*7.3*	-	8.1	4.5	-
Y	21.9	20.0	25.9	20.6	31.2	*29.9*	*21*	33.2	16.5	15.0
U	0.8	0.12	0.9	1.4	4.0	*3.9*	*0.13*	4.8	2.1	0.31
Th	8.3	0.41	9.6	13.1	18.4	*18.3*	*0.39*	20.2	8.1	0.40
Pb	4.0	1.93	7.5	3.6	1.5	*12.0*	*1.89*	9.9	5.5	2.41
Cu	19.7	-	25.8	24.4	87.0	*30.8*	-	54.9	66.3	-
As	0.8	-	15.4	41.9	-	*<0.5*	-	2.4	2.0	-
Zn	49.0	-	44	69	61	*90*	-	104	77	-
Ga	8.2	-	6.2	12.3	13.7	*13.0*		13.6	11.1	-
La	91.4	59.05	68.3	106.9	156.7	*150.0*	*60.0*	160.5	63.0	40.91
Ce	147.5	55.95	130.5	198.9	311.3	*295.2*	*66.5*	318.8	122.1	46.32
Pr	17.45	10.30	14.66	21.98	34.28	*32.24*	-	34.56	13.94	8.22
Nd	61.9	40.60	53.8	81.20	126.4	*119.9*	*54.8*	128.8	50.5	33.12
Sm	8.97	7.93	7.95	6.78	18.62	*17.55*	*8.02*	18.73	7.78	6.84
Eu	2.51	2.48	2.28	3.47	5.10	*4.80*	*2.51*	5.16	2.24	2.21
Gd	6.43	6.99	5.76	8.89	12.77	*12.50*	*7.17*	13.40	5.81	6.32
Tb	0.78	0.885	0.72	1.04	1.56	*1.50*	-	1.65	0.72	0.81
Dy	3.87	3.88	3.39	4.96	7.55	*7.10*	*3.93*	7.65	3.57	3.59
Ho	0.58	0.61	0.47	0.69	1.13	*1.07*	-	1.15	0.54	0.57
Er	1.44	1.26	1.14	1.60	2.55	*2.43*	*1.28*	2.79	1.37	1.20
Tm	0.19	0.15	0.15	0.18	0.32	*0.30*	-	0.36	0.18	0.14
Yb	1.06	0.84	0.74	1.11	1.82	*1.75*	*0.85*	2.00	1.09	0.82
Lu	0.15	0.13	0.10	0.14	0.23	*0.24*	-	0.25	0.14	0.12

Also the pairs of major and trace elements of the glimmeritic rocks exhibit ranges for incompatible elements in-or near the kamafugitic fields (fig. 11). In particular there are apparent correlations between Nd vs. Sm, Th vs. U, La vs. Yb and Sr vs. Rb (Fig. 12); however, correlations are not so evident for the rocks of carbonatitic affinity (cf. Table 12). Zr vs. Cr diagram in the previous figure defines for the glimmeritic rocks a liquid with an initial Zr content of about 240 ppm, similarly to the APIP lithotypes (cf. Gomes and Comin-Chiaramonti, 2005), suggesting, for a comparable mantle source, comparable melting degrees.

Incompatible elements, normalized to a primitive mantle composition (Fig. 13A) for both petrographic associations and single occurrences, show different behaviours. In fact, the glimmeritic rocks, and even the MT-5 alvikitic dyke and the hydrothermalites, displaing a kamafugitic affinity, are characterized by negative anomalies in K, Sr-P, Hf and Ti, and positive ones in Th, La, Nd, Eu, Tb. Ba and Rb show both negative or positive anomaly. On the other hand, the beforsitic rocks exhibit strong negative Rb-Ba anomalies and relative enrichment in Th, U, K, La, Ce.

Chondrite-normalized REE distribution (Fig. 13B) displays similar behaviours with strong LREE/HREE fractionation, i.e. $(La/Yb)_c$: 65.0±1.3 (glimmeritic dykes), 56.6±2.2 (glimmeritic plugs), 90.3±8.7 (rocks with hydrothermalitic tendency), 56.1±11.7 (beforsitic rocks), 76 (rock with alvikitic affinity, MT5), and 40.3±6.9 (carbonate fraction of MT-3 and MT-5 samples). These latter ones also show Eu/Eu* (Sm-Gd normalization) negative anomalies, i.e. 0.29 (MT-3) and 0.47 (MT-%), probably due to previous crystallization of Ca-rich phases (clinopyroxene-amphibole?). Alternatively this behaviour could have been acquired from the country rock during the hydrothermal event.

Considering the high MgO contents, reaching up to 19 wt% in the glimmeritic rocks, the REE distribution likely represents the products of partial melts of a veined mantle source, strongly enriched in incompatible elements and C, H (e.g. phlogopite-amphibole-carbonate-rich veins).

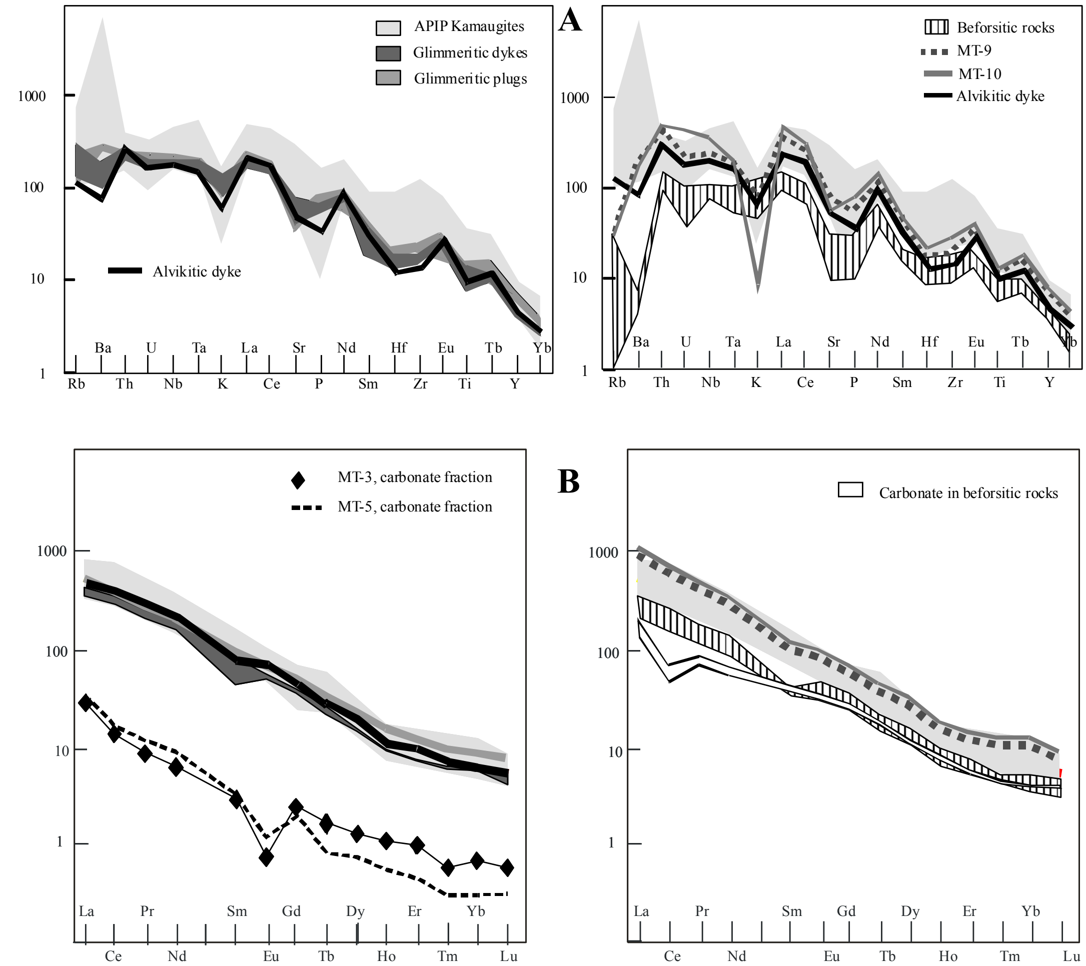

Fig. 13. A) Incompatible elements normalized to primitive mantle concentrations (after Sun & McDonough, 1989). B) Chondrite-normalized (after Boynton, 1984) REE distribution for the various rock types and occurrences from the Planalto da Serra region. Data source in Tables 11 and 12.

ISOTOPIC SYSTEMATICS

Age of the rocks intruding the Rio dos Cavalos Rift.

A complete discussion of this subject is provided by De Min et al. (2013). Here are summarized the main results: $^{40}Ar/^{39}Ar$ (phlogopite and tetraferriphlogopite) yielded an age around 600 Ma (602±16 as average); Rb/Sr systematics, relative to the MT-19 beforsitic rocks (whole rock, carbonate fraction and insoluble residue) defines an isochron Rb/Sr of 598±10 Ma, similar to the Sm/Nd age (errorchron for all the samples) of 601±73. Notably, new data relative to the Rb/Sr systematic (Tables 13 A,B), excluding MT-10 hydrothermalite and MT-16 carbonate fraction, give an age of 599 ± 8 (cf. Fig. 14), confirming the previous dates of De Min et al. (2013).

Concluding, from the available dates, it can be state that the K-alkaline-carbonatitic rock types of the Rio de Cavalos Rift have an age of about 600 Ma, and that this event can be associated with the Brasiliano Cycle (cf. Cordani et al., 2012).

Table 13. A) Rb, Sr contents (ppm), $^{87}Rb/^{86}Sr$ and $^{87}Sr/^{86}Sr$ isotopic ratios for the magmatic rocks from Planalto da Serra. R_0, initial $^{87}Sr/^{86}Sr$ ratios calculated at 600 Ma. WR, whole rock; Cc calcite; IR, insoluble residue; Dol, dolomite; Cc Fr: carbonate fraction.. **B)** Sm, Nd contents (ppm), $^{147}Sm/^{144}$ Nd and $^{143}Nd/^{144}$ Nd isotopic ratios for the same samples. Isotopic ratios were determined at the Department of Mathematics and Geosciences, University of Trieste: NBS987: $^{87}Sr/^{86}Sr$=0.710250 (2σ: 0.000008) n=20; La Jolla: $^{143}Nd/^{144}Nd$=0.511853 (2σ: 0.000015), n=21. Italics: A, Rb/Sr systemayics (MT-19), B, Sm/Nd systematics, data from Table 3 and 4 of De Min et al. (2013), respectively.

A	Rb	Sr	$^{87}Rb/^{86}Sr$	$^{87}Sr/^{86}Sr$	Rock-type	Carbonate vol%	R_0 (600Ma)
MT-1 WR	58.5	909	0.1862	0.708281 (22)	Glimmeritic dyke	8 Cc	0.706688
MT-3 WR	169.7	940	0.5225	0.711106 (24)	Glimmeritic dyke	6 Cc	0.706635
MT-3 Cc Fr	1.675	6310	0.0768	0.707289 (21)			0.706632
MT-5 WR	71.9	1069	0.1946	0.708294 (25)	Alvikitc dyke	51 Cc	0.706628
MT-5 Cc Fr	1.60	2732	0.0017	0.706643 (24)	Alvikitc dyke		0.706629
MT-9 WR	21.8	1665	0.0379	0.707102(25)	Carbonarared dyke	26 Cc	0.706780
MT-10 WR	18.0	1219	0.0427	0.704668 (21)	Hydrothermalite	3 Cc	0.704302
MT-11 WR	18.3	200	0.2648	0.708965 (24)	Beforsitic neck	59 Dol, 3 Cc	0.706700
MT-11 Dol+Cc Fr	0.045	194	0.00067	0.706707 (25)			0.706701
MT-14 WR	18.2	195	0.2701	0.709164 (25)	Beforsitic neck	65 Dol	0.706853
MT-16 WR	153	1067	0.4150	0.709829 (24)	Glimmeritic plug	2 Cc	0.706278
MT-16 Cc Fr	0.15	195	0.0022	0.704525 (23)	Glimmeritic plug		0.704506
MT-16 IR	171	1053	0.4700	0.710310 (32)	Glimmeritic plug		0.706289
MT-19 Dol+Cc Fr	*0.30*	*1526*	*0.0006*	*0.706731 (22)*	Beforsitic neck	51 Dol, 3 Cc	*0.706726*
MT-19 IR	*30.6*	*29.3*	*3.0290*	*0.732567(20)*			*0.706650*
MT-19 WR	*18.5*	*628*	*0.0852*	*0.707450 (20)*			*0.706721*

B	Sm	Nd	147Sm/144Nd	143Nd/144Nd	Initial (600 Ma)	TDM	εSr	εNd
MT-1 WR	15.42	105.7	0.08818	0.512233(21)	0.511886	1071	38.2	0.42
MT-3 WR	*8.70*	*101.1*	*0.05202*	*0.512093(20)*	*0.51189*	*967*	*37.4*	*0.47*
MT3 Cc Fr	*0.58*	*3.82*	*0.09178*	*0.512249(20)*	*0.51189*	*1082*	*37.4*	*0.46*
MT-5 WR	*15.09*	*126.5*	*0.07211*	*0.512172(22)*	*0.51189*	*1017*	*37.3*	*0.47*
MT5 Cc Fr	*0.62*	*5.36*	*0.06992*	*0.512163(25)*	*0.51189*	*1011*	*37.3*	*0.46*
MT-9 WR	*23.29*	*165.4*	*0.08511*	*0.512219(21)*	*0.51188*	*1062*	*39.4*	*0.39*
MT-10 WR	*20.27*	*194.7*	*0.06293*	*0.512133(21)*	*0.51188*	*995*	*4.3*	*0.41*
MT-11 WR	*8.97*	*61.9*	*0.08760*	*0.512229(24)*	*0.51188*	*1071*	*38.3*	*0.39*
MT-11 Cc Fr	*7.93*	*40.60*	*0.11807*	*0.512353(25)*	*0.51189*	*1207*	*38.3*	*0.47*
MT-14 WR	*6.78*	*81.20*	*0.05047*	*0.512084(23)*	*0.51188*	*966*	*40.5*	*0.40*
MT-16 WR	17.55	119.9	0.08848	0.512231(19)	0.51188	1076	32.3	0.36
MT-16 Cc Fr	8.02	54.8	0.08847	0.512227(20)	0.51188	1080	7.2	0.28
MT-19 WR	*7.78*	*50.5*	*0.09313*	*0.512250(20)*	*0.51188*	*1092*	*38.6*	*0.38*
						1054±64		

Sr-Nd isotopes

In general, the high concentration of most I.E. in all the Planalto da Serra rocks suggests that the effects of crustal contamination on the Nd isotopic systems were negligible and that the parental magma compositions are more likely linked to mantle-enriched sources, related to variable degrees of metasomatism (veined mantle). The data are plotted on Fig. 15 (time-integrated ε-notations of Table 13B), being the values concentrated in the enriched quadrant, with εNd = 0.41 ± 0.05 and εSr extending from 4 to 32-41. Notably, the lowest Sr values refer to the hydrothermalite and to the carbonate component (Sr = 195ppm) of a glimmeritic plug (εSr wr = 32) to suggest a reopening of the system by less enriched fluids, rather than a selective crustal contamination.

In any case, the isotopic systematics testify a distribution which appears quite distinct from that corresponding to the APIP kamafugitites, as indicated in the Fig.15.

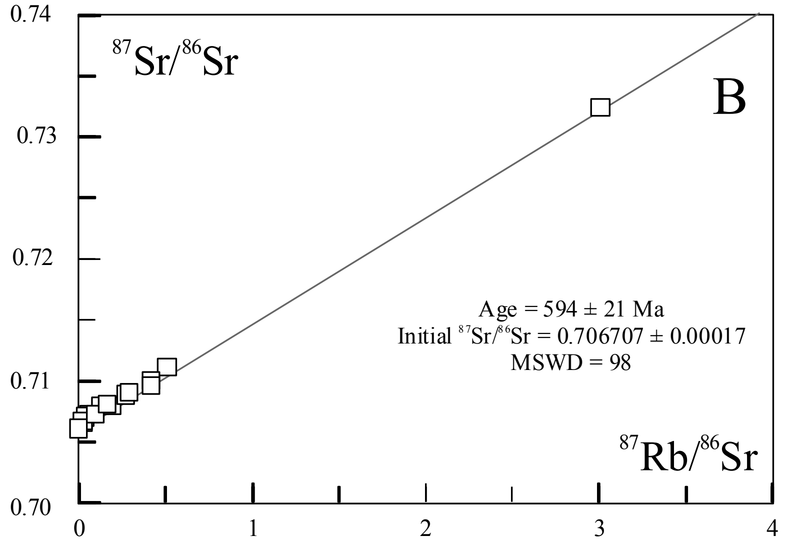

Fig. 14. Errorchron relative to the new data of $^{87}Rb/^{86}Sr$ vs. $^{87}Sr/^{86}Sr$ from the Planalto da Serra samples (cf. Table 13), excluding MT-10 sample and carbonate fraction from MT-16 sample.

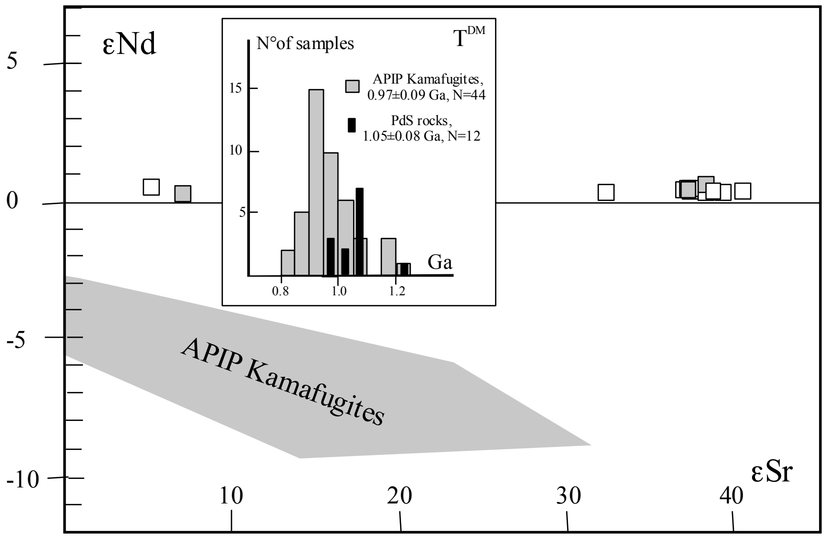

Fig. 15. Time integrated, ε notations, $^{87}Sr/^{86}Sr$ (εSr) vs. $^{144}Nd/^{143}Nd$ (εNd) correlation diagrams. Squares represent the samples from Planalto da Serra (grey squares are the carbonate fractions; cf. Table 13). Grey field represents the composition of APIP kamafugites (Gomes and Comin-Chiaramonti, 2005). **Inset**: histogram relative to the Nd model ages (T^{DM}) for the APIP kamafugites (grey areas) and for Planalto da Serra samples (black areas, PdS); T^{DM} values: calculation of model dates relative to a depleted reservoir, $^{143}Nd/^{144}Nd$=0.513114 and $^{147}Sm/^{144}Nd$=0.222 (cf. Faure, 1986; Dickin, 2005).

Moreover, the almost constant behaviour of the Sm/Nd ratio in the rocks (0.13±0.003; cf. Fig. 12 and Table 13) allows to consider the Nd model ages (De Min et al., 2012) as indicative of the main metasomatic event affecting the lithospheric sources beneath the Planalto da Serra region. These ages (calculated in relation to the depleted mantle, T^{DM}, cf. Table 13; Dickin, 2005) for the whole PdS population (12 samples) fit 1.05±0.08 Ga, roughly similar to those calculated for the APIP kamafugites, i.e. T^{DM} = 0.97±0.09 (44 samples, cf. inset of Fig.15) and Rio Verde-Iporá alkaline province (0.98±0.10, cf. Fig. 1, and Gomes and Comin-Chiaramonti, 2005), defining an Early Neoproterozoic age.

On the other hand, the “uncontaminated trachybasaltic dykes” from the Poxoréu area (cf. Fig. 1

and Gibson et al., 1997) display T^{DM} = 643±52 Ma. Thus, is spite of the different age among the Rio dos Cavalos Rift lithotypes (about 600 Ma) compared to the APIP, Rio Verde-Iporá and Poxoréu rocks (about 84 Ma; cf. Gibson et al., 1995, 1997), the model ages seem to reflect the time when the fluids were "extracted" metasomatizing the lithospheric mantle.

CONCLUDING REMARKS

Along the AZ 125° lineament, where alkaline magmatic rocks are also present in Poxoréu, Rio Verde-Iporá and APIP areas (cf. Fig. 1B), the Rio dos Cavalos Rift, in the Planalto da Serra region, was intruded by dykes and necks of ultramafic and carbonatitic rocks within an extensional zone in the Late-Proterozoic Paraguay mobile belt (Cuiabá Group; cf. Figs. 2 and 3). The Planalto da Serra lithotypes (PdS) are represented by glimmerites of kamafugitic affinity, by carbonatitites having alvikitic and beforsitic characteristics and also by petrographic varieties showing evidences of late hydrothemalization. These hydrothermalization processes, responsible for the lowest isotopic Sr values, suggest that a successive event partially reopened the system by less enriched fluids.

On the whole, the PdS lithologies present petrochemical features similar to those from the Late Cretaceous alkaline rocks from the APIP region. On the other hand they yielded Ar-Ar, Rb/Sr and Sm/Nd similar ages, around 600 Ma. Notably, the 600 Ma date represents an Ediacaran age (630-542 Ma), at the eastern margin of the Amazonian Craton that was fragmented at the beginning of the Neoproterozoic time (cf. Cordani et al., 2012).

The sedimentation of the units of the Paraguay mobile belt occurred in a passive margin, at the onset of the Brasiliano Cycle (cf. Cordani et al., 2009). The whole stratigraphy of the Northern Paraguay Belt is divided into: 1) Alto Paraguay Group, which is the upper unit, 2) the Araras Group, and 3) the Cuiabá Group, the lower unit, which formed presumably between 850 and 600 Ma (Lacerda Filho et al., 2004). According to Alvarenga et al. (2010), the older stratigraphic units of the belt represent the passive margin and the younger ones are typical of a foreland related to the Brasiliano Cycle (cf. Figs 1-3).

As matter of fact, the PdS ultramafic rocks intruding low-grade metasedimentary rocks of the Cuiabá Group indicate that the onset of the deformation and the low-grade metamorphism of the group is older than 600 Ma, and probably taking place at the transition of the Cryogenian and the Ediacaran Periods (630 Ma; cf. Campos Neto et al., 2011).

This age, togheter with other geochronological and tectonic data (cf. Cordani et al., 2012) indicates that it is highly improbable the existence of a large oceanic domain in this area (the Clymine ocean), as postulate by Trindade et al. (2006), and rules out the possible geochronological relationship between the Planalto da Serra intrusions and the alkaline bodies from the Azimuth 125° lineament (Bardet, 1977; Biondi, 2005), which is characterized by the occurrence of ultramafic and alkaline-carbonatite rocks and kimberlites, ranging in age from 80 to 90 Ma.

According to Pimentel et al. (2000), the final amalgamation of Western Gondwana would have occurred at 620 Ma or slightly later, which means that Laurentia, still attached to the Amazonian Craton, was, for a short time, part of the Gondwana Supercontinent. The opening of the Iapetus ocean characterized the separation between Laurentia and the Amazonian Craton. It is unknown when this ocean opened, but it could have been just after 600 Ma. Basins were opened, deformed and metamorphosed around 520 Ma (Trompette, 1997). On the other hand, paleomagnetic measurements indicate that the opening occurred at ca. 580 Ma (Cordani et al., 2009). Taking into account these factors, it is possible that the emplacement of the ultramafic and carbonatitic rocks from Planalto da Serra is related to one of the most important extensional periods of Neoproterozoic times, which is characterized by the separation of Laurentia and the Amazonian Craton.

Considering the Nd model ages (depleted mantle, T^{DM}) as indicative of the main metasomatic events affecting the lithospheric sources beneath the AZ 125° lineament, the values are 1.05±0.07 Ga for the PdS population, 0.97±0.09 Ga for the APIP kamafugites and 0.98±0.10 Ga for the Rio

Verde-Iporá alkaline volcanics, defining on the whole an Early Neoproterozoic age episode, which reflects the time when the fluids were "extracted" metasomatizing the lithospheric mantle.

In conclusion, the T^{DM} model ages suggest that the Planalto da Serra magmas were derived by the remobilization of subcontinental lithospheric mantle that had been enriched by small-volume K-rich melt fractions at the Early to Late Neoproterozoic, well corresponding to the aggregation of Western Gondwana (cf. Scotese, 2009). This severely hampers any hypothesis of mantle plume tail, as proposed by Gibson et al. (1995), given that a subcontinental mantle enrichment, controlled by an Early Neoproterozoic event, produced similar ultramafic alkaline products at 600 and 80-90 Ma.

Acknowledgements

This study is a result of an academic and scientific cooperation agreement between the University of Trieste, Italy (grant MIUR-PRIN 2008), and the University of São Paulo (USP, Brazil). The detailed review and helpful suggestions by Umberto Cordani, Alan Woolley and Gillian Foulger are greatly appreciated. The precious supports of R. Petrini for isotope analyses and of Sandra Andrade for the chemical analyses of carbonate fractions by ICPM are acknowledged. The Brazilian research agencies Fapesp (Proc. 10/50887-3, CBG; 11/50307-0.) and CNPq are also acknowledged for the financial support.

REFERENCES

Almeida, F.F.M., Hasui, Y. (1984). *O Pré-Cambriano do Brasil*. Editora Edgard Blücher. São Paulo, 378p..

Alvarenga, G.J.S. de, Boggiani P.C., Babinski, M., Dardenne, M.A., Figuereido M., Santos, R.V. and Dantas, E.L. (2010). The Amazonian Palaeocontinent. In: Gaucher, C., Sial, A:N:, Halverson, G.P. and Frimmel, H.E. (Eds.) *Neoproterozoic-Cambrian tectonics, global change and evolution: a focus on southwestern Gondwana. Development in Precambrian Geology* **16**, 15-28.

Bailey, S.W. (1984). Classification and structures of the micas. Crystal chemistry of the true micas. *Review in Mineralogy* **13**, 1-60.

Bardet, M.G. (1977). Géologie du diamant. Part 3: gisements de diamants d'Asie, d'Amérique, d'Europe et d'Australasie. *Mémoires du Bureau de Récherches Géologiques et Minières* **83**, 169p.

Barton, M. (1979). A comparative study of some minerals occurring in K-alkaline rocks of the Leucite Hills, Wyoming, The Vico Volcano, Italy, and Toro-Ankole region, Uganda. *Neues Jahrbuch Mineralogische Abhandlungen* **137**, 113-134.

Bellis, A.J. and Canil, D. (2007). Ferric iron in $CaTiO_3$ perovskite as an oxygen barometer for kimberlitic magmas I: experimental calibration. *Journal of Petrology* **48**, 219-230.

Biondi J.C. (2005). Brazilian mineral deposits associated with alkaline and alkaline-carbonatite complexes. In: Comin-Chiaramonti, P., Gomes, C.B. (Eds.) *Mesozoic to Cenozoic alkaline magmatism in the Brazilian Platform*. Edusp/Fapesp, São Paulo, pp. 707-750.

Bizzi, L.A., Araújo, A.L.N. (2005). Dynamics of mantle-derived magmatism in the southwestern São Francisco craton, Brazil. In: Comin-Chiaramonti, P., Gomes, C.B. (Eds.) *Mesozoic to Cenozoic alkaline magmatism in the Brazilian Platform*. Edusp/Fapesp, SãoPaulo, pp. 341-365.

Boctor, N.Z., Boyd, F.R. (1979). Distribution of the rare earth elements in perovskite from kimerlites. *Carnegie Inst. Washington, Ann.Rept.Dir.Geophys.Lab.*, pp. 572-574.

Boggiani, P.C., Alvarenga, G.J.S. (2004). Faixa Paraguay. In: Mantesso-Neto V., Bartorelli A., Carneiro C.D.R., Brito-Neves B.B. (Eds.) *Geologia do Continente Sul-Americano: Evolução da Obra de F.F.M. de Almeida*. Editora Beca, São Paulo, pp. 113-120.

Boynton, W.V. (1984). Cosmochemistry of the Rare Earth elements: meteorite studies. In: Henderson, P. (Ed.) *Rare Earth Element geochemistry*. Elsevier, Amsterdam, pp. 63-114.

Bozhilov, K.N., Jenkins, D.M., Verben, D.R. (2004). Pyribole evolution during tremolite synthesis from oxides. *American Mineralogist* **89**, 74-84.

Brigatti, M.F., Medici, L., Poppi, L., Vaccaro, C. (2001). Crystal chemistry of trioctahedral micas-1M from the Alto Paranaíba Igneous Province, Southeastern Brazil. *Canadian Mineralogist* **39**, 1333-1345.

Campos Neto, M.C., Basei, M.A.S., Janasi V.A., Moraes, R. (2011). Orogen migration and tectonic setting of the Andrelândia Nappe system: an Ediacaran western Gondwana collage, south of São Francisco craton. *Journal of South American Earth Sciences* **24**, 1-14.

Canil, D., Bellis, A.J. (2007). Ferric iron in $CaTiO_3$ perovskite as an oxygen barometer for kimberlite magmas II: applications. *Journal of Petrology* **48**, 231-252.

Carmichael, I.S.E. (1967). The iron-titanium oxides of salic volcanic rocks and their associated ferro-magnesian silicates. *Contributions to Mineralogy and Petrology* **5**, 310-357.

Černy, Y.P., Ercit, T.S. (1986). Mineralogy of niobium and tantalum. Crystallochemical relationships, paragenetic aspects and their economic implications. In: Moeller, P., Èerny, P., Sanpe, F. (Eds.) *Lantanides, tantalum and niobium. Special Publication of Society for Geology Applied to Mineral Deposits* **7**, 27-79.

Chakhmouradian, A.R., Mitchell, R.H. (2001). Three compositional varieties of perovskite from kimberlites of the Lac de Gras field (Northwest Territories, Canada). *Mineralogical Magazine* **65,***133-148.*

Comin-Chiaramonti, P., Gomes, C.B. (1995). *Alkaline magmatism in central-eastern Paraguay. Relationships with coeval magmatism in Brazil.* Edusp/Fapesp, São Paulo, 464p.

Comin-Chiaramonti, P., Gomes, C.B. (2005). *Mesozoic to Cenozoic alkaline magmatism in the Brazilian Platform*. Edusp/Fapesp, São Paulo, 752p.

Comin-Chiaramonti P., Gomes C.B., Marques L.S., Censi P., Ruberti E., Antonini P. (2005). Carbonatites from southeastern Brazil: geochemistry, O-C, Sr-Nd-Pb isotopes and relationships with the magmatism from the Paraná-Angola-Namibia Province. In: Comin-Chiaramonti, P., Gomes, C.B. (Eds.) *Mesozoic to Cenozoic alkaline magmatism in the Brazilian Platform*. Edusp/Fapesp, SãoPaulo, pp. 651-682.

Cordani, U.G., Pimentel, M.M., Araújo, C.E.G.; Basei, A.S., Fuck, R.A., Girardi, V.A.V. (2012). Was there an Ediacaran Clymene Ocean in Central South America? *American Journal of Sciences*, submitted.

Cordani U.G., Teixeira W., D'Agrella-Filho M.S., R.I.Trindade R.I. (2009). The position of the Amazonian Craton in supercontinents. *Gondwana Research* **15**, 396-407.

Dantas, E. L., Armstrong, R., Pimentel, M.M., Fuck, R., Martinelli, C., Silva, M.F., Laux, J.H. (2007). 800 Ma rifting in the Paraguay Belt, central Brazil: U-Pb SHRIMP age determination, Rodinia break-up and implications for a connection with Avalonian peri-Gondwana terranes. *Geological Society of America, Abstract with Programs* **39**, p. 622.

Deer, R.W., Howie, R.A., Zussman, J. (1992). *An introduction to the rock-forming minerals.* Longman Group UK Limited, London, 696p.

De Min, A., Hendriks, B.W.H., Slejko, F., Comin-Chiaramonti, P., Girardi, V.A.V., Ruberti, E., Gomes, C.B., Neder, R.D., Pinho, F.E.C. (2013). Age of ultramafic high-K rocks from Planalto da Serra (Mato Grosso, Brazil). *Journal of South American Earth Sciences* (in press).

DePaolo, D. J. (1988). *Neodymium isotope geochemistry, an introduction*. Berlin: Springer-Verlag, pp. 33-39.

Dickin, A.P. (2005). *Radiogenic isotope geology*, 2nd ed. Cambridge University Press, Cambridge, pp. 76-77.

Faure, G. (1986). *Principles of isotope geology*. John Wiley & Sons, New York, 589p.

Foley, S.F., Venturelli, G., Green, D.H., Toscani, L. (1987). The ultrapotassic rocks: classification and constraints for petrogenetic models. *Earth-Science Reviews* **24**, 81-134.

Galle, O.K., Runnels, R.T. (1960). Determination of CO_2 in carbonate rocks by controlled loss on ignition. *Journal of Sedimentary Research* **30**, 613-618.

Gibson, S.A., Thompson, R.N., Leonardos, O.H., Dickin, A.P., Mitchell, J.G. (1995). The Late Cretaceous impact of the Trindade mantle plume: evidence from large-volume, mafic, potassic magmatism in SE Brazil. *Journal of Petrology* **36**, 189-229.

Gibson, S.A., Thompson, R.N., Weska, R., Dickin, A.P., Leonardos, O.H. (1997). Late Cretaceous rift-related upwelling and melting of the Trindade starting mantle plume head beneath western Brazil. *Contributions to Mineralogy and Petrology* **126**, 303-314.

Gomes C.B., Comin-Chiaramonti P. (2005). Some notes on the Alto Paranaíba igneous province. In: Comin-Chiaramonti, P., Gomes, C.B. (Eds.) *Mesozoic to Cenozoic alkaline magmatism in the Brazilian Platform*. Edusp/Fapesp, SãoPaulo, pp. 317-340.

Heinz, M., Debayle, E., Vauchez, A. (2005). Upper mantle structure of the South American continent and neighboring oceans from surface wave tomography. *Tectonophysics* **406**, 115-139.

Jenkins, D.M., Holland, T.J.B., Clare, A.K. (1991). Experimental determination of the pressure-temperature stability field and thermochemical properties of synthetic tremolite. *American Mineralogist* **76**, 458-469.

Kopylova1, M.G., Mogg, T:, Smith, B.S. (2010). Mineralogy of the Snap Lake kimberlite, Northwest Territories, Canada, and the compositions of phogopite as records of its crystallization. *Canadian Mineralogist* **48**, 549-570.

Kjarsgaard, B.A. (1998). Phase relations of a carbonated high-CaO nephelinite at 0.2 and 0.5 GPa. *Journal of Petrology* **39**, 2061-2075.

Lacerda Filho, J.V, Abreu Filho, W., Valente, C.R., Oliveira, C.C., Albuquerque, M.C. (2004). Geologia e Recursos Minerais do Estado de Mato Grosso. Programa Integração, Atualização e Difusão de Dados da Geologia do Brasil, Subprograma mapas geológicos estaduais, Escala 1:1000.000. Goiânia: CPRM, 2004 (Convênio CPRM/SICME), 200p. + mapas geológicos.

Leake, B.E.,.Woolley, Arps C.E.S., Birch, W., Gilbert, M. C., Grice J.D., Hawthorne, F. C., Kato, A., Kisch, H., Krivovichev, V.G., Linthout, K., Laird, J., Mandarino, J., Maresch, W.V., Nickel, E.H., .Rock, N.M.S., Schumacher, J.C., Smith, D.C., Stephenson, N.C.N., Ungaretti, U., Whittaker. E.J., Youzhi, G. (1997). Nomenclature of amphiboles: report of the subcommittee on amphiboles of the International Mineralogical Association, commission on new minerals and mineral names. *Canadian Mineralogist* **35**,.219-246.

Manzano, J.C., Godoy, A.M., Araújo, L.M.B. (2008). Contexto tectônico dos granitóides da faixa de dobramentos Paraguay, MS e MT. *Geociências* **27,** 493-507.

Melluso, L., Lustrino, M., Ruberti, E., Brotzu, P., Gomes, C.B., Morbidelli, L., Morra, V., Svisero, D.P., d'Amelio, F. (2008). Major- and trace-element composition of olivine, perovskite, clinopyroxene, Cr-Fe-Ti oxides, phlogopites and host kamafugites and kimberlites, Alto Paranaíba, Brazil. *The Canadian Mineralogist* **46**, 19-40

McGee, B., Collins, A.S., Trindade, R.I.F. (2012). G'day Gondwana - the final accretion of as upercontinent: U-Pb ages from the post-orogenic São Vicente Granite, northern Paraguay Belt, Brazil. *Gondwana Research* **21**, 316-322.

Mitchell, R.H., Bergmann, S.C. (1991). *Petrology of lamproites.* Plenum Press, New York, 447p.

Morimoto, N. (1988). Nomenclature of pyroxenes. *Mineralogical Magazine* **52**, 535-550.

Ormond, M.M.S. (2006). *Petrografia do complexo alcalino de Planalto da Serra e estudo geológico e geoquímico da intrusão Chibata-Denizar.* Trabalho de conclusão de curso, Universidade Federal de Mato Grosso, Cuiabá, 149p. (unpublished).

Pimentel, M.M., Fuck, R.A., Jost, H., Ferreira Filho, C.F., Araújo, S.M. (2000). The basement of the Brasília Fold Belt and the Goiás Magmatic Arch. In: Cordani, U.G., Milani, E.J., Thomaz Filho, A., Campos, D.A. (Eds.) *Tectonic evolution of South America. 31st International Geological Congress, Rio de Janeiro,* pp. 195-229.

Riccomini, C., Nogueira A.C.R., Sial, A.N. (2007). Carbon and oxygen isotope geochemistry of Ediacaran outer platform carbonates, Paraguay Belt, central Brazil. *Anais da Academia Brasileira de Ciências* **79**, 519-527.

Robinson, P., Spear, F. S., Schumacher, J. C., Laird, J., Klein, C., Evans, B. W., Doolan, B. L. (1982). Phase relations of metamorphic amphiboles: natura occurrence and theory. In: Veblen, D.R., Ribbe, P.H. (Eds.) *Amphiboles: petrology and experimental phase relations*. *Mineralogical Society of America, Review in Mineralogy* **9B**, 1-128.

Scordari, F., Schinfaro, E., Lacalamita, M., Mesto, E. (2012). Crystal chemistry of trioctahedral micas-2M_1 from Bunyaruguru kamafugite (southwest Uganda). *American Mineralogist* **97**, 430-439

Scotese, C.R (2009). Late Proterozoic plate tectonics and palaeogeography: a tale of two supercontinents, Rodinia and Pannotia. *Geological Society, London, Special Publication* **326**, 67-83.

Simandl, G.J., Jones, P.C., Rotella M. (2001). Blue river carbonatites, British Columbia. Primary exploration for tantalum. *Exploration and Mining in British Columbia*, pp.123-132.

Sousa, M.Z.A., Ruberti, E:, Comin-Chiaramonti, P., Gomes, C.B. (2005). Alkaline magmatism from the Mato Grosso State, Brazil: the Ponta do Morro complex. In: Comin-Chiaramonti, P., Gomes, C.B. (Eds.) *Mesozoic to Cenozoic alkaline magmatism in the Brazilian Platform*. Edusp/Fapesp, São Paulo, pp. 241-260.

Sun, S.-S., McDonough, W.F. (1989). Chemical and isotopic systematics of oceanic basalts: implications for mantle composition and processes. In: Saunders, A.D., Norry, M.J. (Eds.) *Magmatism in the ocean basins*. *Geological Society of London, Special Publication* **42**, 313-345.

Thompson, R.N., Gibson, S.A., Mitchell, J.G., Dickin, A.P., Leonardos, O.H., Brod, J.A., Greenwood, J.C. (1998). Migrating Cretaceous-Eocene magmatism in the Serra do Mar Alkaline Province, SE Brazil: melts from the deflected Trindade mantle plume? Journal of Petrology **39**, 1493-1526.

Tohver, E., Trindade, R.I.F., Solum, J.C., Hall, C.M., Riccomini, C., Nogueira, A.C. (2010). Closing the Clymene ocean and bending a Brasiliano belt: evidence for the Cambrian formation of Gondwana, southeast Amazon craton. *Geological Society of America*. *Geology* **38**, 267-270.

Tomkins, L.A., Bailey, S.W., Haggerty, S.E. (1984). Kimberlitic chlorites from Sierra Leone, West Africa: unusual chemistries and structural polytipes. *American Mineralogist* **69**, 237-249.

Traversa, G.; Gomes, C.B.; Brotzu, P.; Buraglini, N.; Morbidelli, L.; Principato, M.S.; Ronca, S.; Ruberti, E. (2001). Petrography and mineral chemistry of carbonatites and mica-rich rocks from the Araxá complex (Alto Paranaíba Province, Brazil). *Anais da Academia Brasileira de Ciências* **73**, 71-98.

Trindade, R.I.F., Font, E., D'Agella-Filho, M.S., Nogueira, A.C.R., Riccomini, C. (2003). Low-latitude and multiple geomagnetic reversal in the Neoproterozoic Puga cap carbonate, Amazon craton. *Terra Nova* **15**, 441-446.

Trompette, R. (1997). Neoproterozoic (~600 Ma) aggregation of Western Gondwana: a tentative scenario. *Precambrian Research* **82**, 101-112.

Welch, M.D., Pawley, R. (1991). Tremolite: new enthalpy and entropy data from a phase equilibrium study of the reaction tremolite=2diopside+1.5orthoenstatite+β-quartz+H_2O. *American Mineralogist* **76**, 1931-1939.